Studies on genetic polymorphisms of host cell receptors affecting viral entry into cells

（ウイルスの細胞侵入に影響を及ぼす宿主細胞受容体の遺伝子多型に関する研究）

Takanari HATTORI

CONTENTS

Abbreviations

ACE2	angiotensin-converting enzyme 2
αDG	α-dystroglycan
B	benign
CADD	combined annotation dependent depletion
cDNA	complementary DNA
CLD	collectrin-like domain
COVID-19	coronavirus disease 2019
CoVs	coronaviruses
cryo-EM	cryo-electron microscopy
CT	cytoplasmic tail
D	deleterious
DAPI	4,6-diamidino-2-phenylindole
dbSNP	Single Nucleotide Polymorphism Database
DMEM	Dulbecco's modified Eagle's medium
DNA	deoxyribonucleic acid
EBOV	Ebola virus
EDTA	ethylenediaminetetraacetic acid
ExAC	Exome Aggregation Consortium
FCS	fetal calf serum
FITC	fluorescein isothiocyanate
G	glycoprotein of VSIV
genomAD	Genome Aggregation Database
GFP	green fluorescent protein
GP	glycoprotein
HEK	human embryonic kidney
HRP	horseradish peroxidase
hTIM-1	human TIM-1
HU	Hokkaido University
IgG	immunoglobulin G
IgV	immunoglobulin variable
IIZC	International Institute for Zoonosis Control

IUs	infectious units
JUNV	Junin virus
LASV	Lassa virus
LB	likely benign
LD	likely deleterious
LDC	likely disease-causing
LLOV	Lloviu virus
MAF	minor allele frequency
MARV	Marburg virus
MERS-CoV	Middle East respiratory syndrome coronavirus
MFI	mean fluorescence intensity
MILIBS	metal-ion-dependent ligand binding site
MLD	mucin-like domain
NCBI	National Center for Biotechnology Information
ND	neck domain
PAGE	polyacrylamide gel electrophoresis
PBS	phosphate buffered saline
PBST	PBS containing 0.05% Tween 20
PCR	polymerase chain reaction
PD	protease domain
PDB	Protein Data Bank
PolyPhen-2	polymorphism phenotyping 2
PosD	possibly damaging
ProD	probably damaging
PS	phosphatidylserine
RBD	receptor binding domain
REVEL	rare exome variant ensemble learner
RIPA	radioimmunoprecipitation assay
RNA	ribonucleic acid
S	spike
SARS-CoV	severe acute respiratory syndrome coronavirus
SDs	standard deviations

SDS	sodium dodecyl sulfate
SIFT	sorting intolerant from tolerant
SNPs	single nucleotide polymorphisms
SNVs	single nucleotide variants
SP	signal peptide
T	tolerated
TAM	Tyro3/Axl/Mer
TIM	T-cell immunoglobulin mucin
TM	transmembrane domain
TMPRSS2	transmembrane protease serine 2
TOPMed	Trans-Omics for Precision Medicine
VOCs	variants of concern
VSIV	vesicular stomatitis Indiana virus
WHO	World Health Organization
WISE	World-leading Innovative and Smart Education
WT	wildtype

Notes

The contents of Chapter I have been published in Microbiology Spectrum.

Hattori T, Saito T, Okuya K, Takahashi Y, Miyamoto H, Kajihara M, Igarashi M, and Takada A. Human ACE2 genetic polymorphism affecting SARS-CoV and SARS-CoV-2 entry into cells. Microbiology Spectrum, 10(4), e0087022, 2022.

The contents of Chapter II have been published in Viruses.

Hattori T, Saito T, Miyamoto H, Kajihara M, Igarashi M, and Takada A. Single nucleotide variants of the human TIM-1 IgV domain with reduced ability to promote viral entry into cells. Viruses, 14(10), 2124, 2022.

Preface

In recent years, emerging and re-emerging infectious diseases in humans have been increasingly reported. Viral infectious diseases have particularly caused frequent outbreaks worldwide and become public health threats in the past several decades. For instance, three coronaviruses (CoVs), represented by severe acute respiratory syndrome coronavirus (SARS-CoV), SARS-CoV-2, and Middle East respiratory syndrome coronavirus (MERS-CoV) were associated with emerging viral pneumonia in humans, and SARS-CoV-2 caused a pandemic that has made a significant impact on global health. Hemorrhagic fever viruses including filoviruses, arenaviruses, bunyaviruses, and flaviviruses have also continuously produced outbreaks in many countries. Of these, filoviruses such as Ebola virus (EBOV) and Marburg virus (MARV) causing Ebola virus disease and Marburg virus disease, respectively, and arenaviruses such as Lassa virus (LASV) and Junin virus (JUNV) causing Lassa fever and Argentine hemorrhagic fever, respectively, are known to cause severe febrile diseases in humans with high mortality rates. However, interestingly, some clinical cases of these virus infections are reported to be potentially asymptomatic or associated with only mild symptoms in the previous outbreaks [1–4]. Considering these differences in the disease symptom and severity among individuals, host genetic polymorphisms in humans are suggested to be one of the factors determining the pathogenesis of viral infections. In other words, genetic polymorphisms in humans might be important for differential susceptibility or resistance to viral infections. However, the information on this topic is still limited.

In general, the genetic polymorphisms are reported to be associated with the genetic diversity and individuality in the population, susceptibility or resistance to diseases, and response to medicine [5,6]. Among the genetic polymorphisms, single nucleotide substitutions have been well investigated and the information has been accumulated in public databases. They are known as rare single nucleotide variants (SNVs; defined as deoxyribonucleic acid [DNA] sequence variation that occurs when a single nucleotide in the genome sequence is altered with a frequency less than 1%) or single nucleotide polymorphisms (SNPs; defined as point mutations with the minor allele frequency greater than 1% in the population). When nonsynonymous SNV/SNP substitutions are present within exons of host genomic DNA, which are gene regions encoding proteins, polymorphisms of a host protein gene have potential to influence protein structure and function and have been shown to affect the susceptibilities of hosts and/or severity of viral infectious diseases [7–10].

Enveloped viruses have the nucleocapsid containing their viral genomes in a lipid bilayer, which is derived from the host cell membrane, associated with viral envelope

glycoproteins responsible for viral entry into cells. The viral membrane often contains phosphatidylserine (PS), which is one of the phospholipids consisting of the host cell membrane. These membrane surface properties of virus particles are determined thorough virus budding from infected host cells. Viral attachment to target cell surfaces is the first step of viral infection. Viral surface glycoproteins on the envelope bind to host cell receptors specific for respective viruses, leading to viral entry into cells, and subsequently induces fusion between the viral envelope and the host cell membrane. Some viruses utilize multiple receptors during the cellular entry process (e.g., attachment receptors and fusion receptors).

The entry of SARS-CoV-2 into cells is initiated by the interaction of its envelope glycoprotein with several host receptors (e.g., angiotensin-converting enzyme 2 [ACE2], neuropilin-1, C-type lectins, and PS receptors) on the cell membrane, and proteolytic processing of the viral glycoprotein with host proteases such as furin and transmembrane protease serine 2 (TMPRSS2) is required for efficient membrane fusion during the entry [11]. The EBOV glycoprotein is also known to bind to multiple receptors; C-type lectins, integrin α5β1, and PS receptors as attachment receptors and Niemann-Pick C1 as the only known fusion receptor [12]. PS receptors, including T-cell immunoglobulin mucin (TIM) family (TIM-1, TIM-3, and TIM-4) and Tyro3/Axl/Mer (TAM) family, are reported to mediate the binding to PS on the viral envelope and to promote infections of enveloped viruses such as filoviruses, arenaviruses, and flaviviruses in a manner independent of specific receptor recognition by their envelope glycoproteins [13]. In the present thesis, I focus on SNVs of two host cell receptors (i.e., ACE2 and TIM-1) on the cellular entry of SARS CoVs and filoviruses/arenaviruses, respectively. SNV substitutions of these receptors might influence susceptibility of humans to these viruses, whereas the information on SNVs affecting the receptor function is still limited.

The purpose of this study is to investigate the genetic polymorphisms of host cell receptors affecting viral entry into cells. To focus on the viral entry step, I employed pseudotyped vesicular stomatitis Indiana virus (VSIV) and analyzed SNVs in ACE2 and TIM-1 receptors. In Chapter I, I investigated the effects of human ACE2 SNV substitutions on cell susceptibilities to SARS-CoVs, including SARS-CoV-2 variants of concern (VOCs). In Chapter II, I focused on SNVs of human TIM-1 affecting the susceptibilities to filoviruses and arenaviruses. The present data suggest that SNVs of these host cell receptors affect cell susceptibilities to the viruses and provide evidence of the potential impact of SNVs on individual differences in susceptibilities to viral infections.

Chapter I

Human ACE2 genetic polymorphism affecting SARS-CoV and SARS-CoV-2 entry into cells

Introduction

Coronaviruses (CoVs), which belong to the family *Coronaviridae* in the order *Nidovirales*, are enveloped positive-sense single-stranded ribonucleic acid (RNA) viruses. The genus *Betacoronavirus* is one of the four genera in the subfamily *Orthocoronavirinae* and includes severe acute respiratory syndrome coronavirus (SARS-CoV), SARS-CoV-2, and Middle East respiratory syndrome coronavirus, all of which are known to cause severe pneumonia in humans. Since its first report in China, coronavirus disease 2019 (COVID-19) caused by SARS-CoV-2 has spread all over the world. As of 2 March 2022, there have been 650,332,899 confirmed cases of COVID19, including 6,649,874 deaths, as indicated by the World Health Organization (WHO) COVID-19 report (https://covid19.who.int/), accessed on 22 December 2022.

The spike (S) protein of SARS-CoV and SARS-CoV-2 is a single envelope glycoprotein that is responsible for virus entry into cells and thought to be important for host range restriction of these CoVs [14,15]. The S protein is the primary determinant of antigenicity and thus the only target of neutralizing antibodies [14,15]. The mature S protein consists of two subunits, S1 and S2, which are cleaved by host proteases during the post translational processing [11]. The S1 subunit contains the receptor binding domain (RBD), which recognizes angiotensin-converting enzyme 2 (ACE2) as a receptor, leading to viral attachment to the host cell [11]. Subsequently, the S2 subunit is further cleaved at the S1/S2 and S2' sites by host proteases such as furin, transmembrane protease serine 2 (TMPRSS2), and cathepsins on the surface and in the endosomes of target cells. After the cleavage of the S protein, the S2 subunit induces membrane fusion between the viral envelope and host cell membranes [16,17].

During the current SARS-CoV-2 pandemic, some particular SARS-CoV-2 lineages are classified as variants of concern (VOCs), such as the Alpha (lineage B.1.1.7), Beta (lineage B.1.351), Gamma (lineage P.1), Delta (lineage B.1.617.2), and Omicron (lineage B.1.1.529) variants, which are thought to be associated with increased transmissibility and infectivity [18,19]. Focusing on the mutations in the RBD of these four VOCs (Alpha, Beta, Gamma, and Delta), the N501Y mutation found in the Alpha variant, K417N, E484K, and N501Y mutations found in the Beta variant, K417T, E484K, and N501Y

mutations found in the Gamma variant, and L452R and T478K mutations found in the Delta variant are reported to enhance the binding affinity of the S protein to the ACE2 receptor and also to be important for escape from neutralization by several monoclonal antibodies [20].

The severity of COVID-19 symptoms differs among individuals, ranging from asymptomatic or only mild cold-like symptoms to pneumonia with a severe clinical course [1]. While the pathogenesis of COVID-19 is thought to be related to viral tropism, host cell-mediated immunity, and the inflammatory response [21], host genetic polymorphisms in humans have also been suggested to be one of the factors determining the disease severity of SARS-CoV-2 infection [22]. Since ACE2 is the key functional host receptor for SARS-CoV-2, genetic diversity in this receptor may potentially be involved in the difference of SARS-CoV-2 infectivity among individuals. ACE2 is expressed in various tissues, including lung, kidney, intestine, and blood vessels [23] and plays an important role in controlling blood pressure by regulating the renin-angiotensin-aldosterone system [24]. Several studies have suggested that single nucleotide variants (SNVs) including single nucleotide polymorphisms (SNPs) in ACE2 could potentially change the efficiency of SARS-CoV-2 infection by affecting the affinity of ACE2 to the SARS-CoV-2 S protein or the cell surface expression of ACE2 [25–27]. Another group examined the impact of eight ACE2 SNVs found in specific populations focusing on the cellular entry of SARS-CoV-2, and suggested that these SNV substitutions had limited impact on the efficiency of ACE2-mediated entry of SARS-CoV-2 [28]. However, many ACE2 SNVs remain to be investigated to determine their importance for SARS-CoV-2 infection.

Using a deep mutational scanning method, a previous study showed the effects of 117 single amino acid substitutions of ACE2, all located on the interface with the SARS-CoV-2 S protein, which are present in the angiotensin peptide-binding cavity [29]. Of these, 31 ACE2 SNV substitutions were found to affect the binding affinity of ACE2 to the RBD of the SARS-CoV-2 S protein [29,30]. However, it is still unknown whether these SNV substitutions affect cell susceptibilities to the virus. In this chapter, I virologically analyzed the impact of the ACE2 SNVs on the cellular entry of SARS-CoV and SARS-CoV-2 using vesicular stomatitis Indiana viruses (VSIVs) pseudotyped with the S protein. Four SARS-CoV-2 VOCs were also investigated. The obtained data suggest that ACE2 SNVs may potentially influence host susceptibilities to SARS-CoV and SARS-CoV-2, including VOCs.

Materials and Methods

ACE2 SNVs information

Based on previous studies [29,30], 29 SNV substitutions in ACE2 were selected for the analysis. The allele frequencies of ACE2 SNVs were extracted from Trans-Omics for Precision Medicine (TOPMed), Exome Aggregation Consortium (ExAC), or Genome Aggregation Database (gnomAD) linked with the Single Nucleotide Polymorphism Database (dbSNP) on the National Center for Biotechnology Information (NCBI) website [31]. The NCBI ID numbers of these SNVs are as follows: rs73635825 (S19P), rs1244687367 (I21T), rs756231991 (E23K), rs1434130600 (A25T), rs4646116 (K26R), rs781255386 (T27A), rs778500138 (E35D), rs1348114695 (E35K), rs146676783 (E37K), rs1192192618 (Y50F), rs760159085 (N51D), rs1325542104 (M62V), rs1199100713 (N64K), rs755691167 (K68E), rs1256007252 (F72V), rs867318181 (E75G), rs766996587 (M82I), rs763395248 (T92I), rs1395878099 (Q102P), rs759579097 (G326E), rs143936283 (E329G), rs370610075 (G352V), rs961360700 (D355N), rs142984500 (H378R), rs751572714 (Q388L), rs762890235 (P389H), rs1016409802 (H505R), rs1352194082 (R514G), and rs1263424292 (Y515C). In the present study, the most common genotype of human ACE2 in the global population was defined as wildtype (WT) (GenBank accession number, NM_021804.3) based on the genetic information from NCBI.

Cells

Human hepatoma Huh-7 and human embryonic kidney (HEK) 293T cells were cultured in Dulbecco's modified Eagle's medium (DMEM) (Sigma-Aldrich) containing 10% fetal calf serum (FCS) (Cell Culture Bioscience), 100 U/ml penicillin, and 0.1 mg/ml streptomycin (Gibco) at 37°C in a 5% CO_2 incubator.

Plasmids

Total RNA was extracted from Huh-7 cells with Trizol (Invitrogen) and then a complementary DNA (cDNA) library was prepared using SuperScript^{TM} IV (Invitrogen) and an ACE2 gene specific primer (5'-CTAAAAGGAGGTCTGAACATCATCAGTGTT-3'). The coding region of the human ACE2 gene was amplified by polymerase chain reaction (PCR) using the primers SacI-ACE2-F (5'-GCGGAGCTCGCCACCATGTCAAGC-3') containing a SacI restriction site and NheI-ACE2-R (5'-CGCGCTAGCAAAGGAGGTCTGAAC-3') containing an NheI restriction site. After sequence confirmation of the WT human ACE2 gene, this PCR product was inserted into a plasmid, pCAGGS, to express full-length ACE2 fused with a

C-terminal 3 × FLAG tag (pCAGGS-ACE2 3×FLAG). SNV mutants were produced by site-directed mutagenesis using KOD One polymerase (TOYOBO) with primers containing the desired nucleotide substitutions. All mutations were confirmed by Sanger sequencing of the plasmids. Generation of the recombinant plasmids and proteins was approved by Hokkaido University Safety Committee for Genetic Recombination Experiments (21[4]).

VSIVs pseudotyped with S proteins of SARS CoVs

Using a replication-incompetent VSIV containing the green fluorescent protein (GFP) instead of the receptor-binding VSIV glycoprotein (G) gene (VSIVΔG*-G), VSIVs pseudotyped with S proteins of SARS CoVs (VSIVΔG*-SCoV and VSIVΔG*-SCoV-2) were generated as described previously [32,33]. Briefly, 24 hours after transfection of HEK293T cells with pCAGGS expressing the S protein of SARS-CoV (Tor2 strain: GenBank accession number, NC_004718.3) or SARS-CoV-2 (strain WHU01: GenBank accession number MN988668.1), the cells were incubated with VSIVΔG*-G for 60 min at 37°C. After washing three times with DMEM, the medium was replaced by DMEM with 10% FCS. Twenty-four hours later, the supernatants were harvested and stored at -80°C until use. Virus infectious units (IUs) in HEK293T cells were determined by counting the number of GFP-positive cells with an IN Cell Analyzer 2500HS (GE Healthcare). To produce VSIVs pseudotyped with the S proteins having the substitutions in RBD derived from the Alpha (N501Y), Beta (K417N, E484K, and N501Y), Gamma (K417T, E484K, and N501Y), and Delta (L452R and T478K) variants, the mutant S protein genes were constructed by site-directed mutagenesis with KOD One (TOYOBO) based on the S protein gene of SARS-CoV-2 WHU01, which is an early isolate from Wuhan. Each mutation was confirmed by Sanger sequencing. The use of VSIVs was approved by the Committee for Safety Management of Pathogens, Research Center for Zoonosis Control, Hokkaido University (10[06]), Hokkaido University Safety Committee for Genetic Recombination Experiments (21[4]), and the Ministry of Education, Culture, Sports, Science, and Technology, Japan.

Sodium dodecyl sulfate-polyacrylamide gel electrophoresis (SDS-PAGE) and Western blotting

To check the expression levels of the ACE2 WT and SNV mutant proteins, HEK293T cells were transfected with expression plasmids encoding 3 × FLAG-tagged ACE2 proteins or empty pCAGGS as a negative control. At 48 hours post-transfection, these cells were washed with phosphate-buffered saline (PBS) three times and lysed with

a radioimmunoprecipitation assay (RIPA) buffer (0.25 mM ethylenediaminetetraacetic acid [EDTA] pH 8.0, 25 mM Tris/HCl pH 7.6, 150 mM NaCl, 1% NP-40, 1% sodium deoxycholate, 0.1% SDS). Then, the supernatants were collected after centrifugation. Each sample was mixed with 4 × sample buffer (Bio-Rad) with 5% 2-mercaptoethanol, and solubilized proteins were separated by 10% SDS-PAGE. Separated proteins were then blotted on a polyvinylidene difluoride membrane (Merck Millipore Corporation). After blocking with 5% skim milk, the membrane was incubated with a mouse anti-FLAG M2 monoclonal antibody (F1804, Sigma-Aldrich) or mouse anti-β-actin monoclonal antibody (AC15, Abcam) as a primary antibody for 1 hour. After washing with 0.05% Tween 20 in PBS (PBST), the membrane was incubated with horseradish peroxidase (HRP)-conjugated goat anti-mouse immunoglobulin G (IgG) (115-035-062, Jackson ImmunoResearch) as a secondary antibody for 1 hour. After washing with PBST, the bound antibodies were visualized with Immobilon Western (Merck Millipore Corporation). Unglycosylated and glycosylated forms of the ACE2 protein were detected as approximately 85 kD and 110-120 kD bands in consistent with a previous study, respectively [34,35]. The relative expression levels were analyzed using Amersham Imager 600 (GE Healthcare).

Virus entry assay

HEK293T cells, which are known to lack expression of endogenous ACE2 [36], were seeded in 96-well plates (1.0×10^4 cells per well) precoated with poly-L-lysine (Cultrex, R&D Systems). Twenty-four hours later, the cells were transfected with 0.2 μg/well pCAGGS encoding FLAG-tagged ACE2 WT or SNV mutant proteins using TransIT-LT1 (Mirus). At 24 hours post-transfection, these cells were infected with VSIVΔG*-SCoV, VSIVΔG*-SCoV-2, or VSIVΔG*-G. Each virus was appropriately diluted to provide 300-400 IUs/well in HEK293T expressing WT ACE2. VSIVΔG*-SCoV and VSIVΔG*-SCoV-2 were treated with an anti-VSIV G monoclonal antibody (VSIV-G (N) 1-9) to abolish the background infectivity of parental VSIVΔG*-G [37]. Twenty-four hours later, IUs were determined by counting the numbers of GFP-expressing cells using an IN Cell Analyzer 2500HS (GE Healthcare). The relative infectivity was determined by setting the value of cells expressing ACE2 WT to 100%.

Immunofluorescence assay

HEK293T cells were seeded in a μ-Slide 8 Well Chamber Slide (iBidi GmbH) after precoating with poly-L-lysine (Cultrex, R&D Systems). Twenty-four hours later, the cells were transfected with the pCAGGS encoding FLAG-tagged ACE2 proteins or empty

pCAGGS. At 24 hours post-transfection, the cells were washed with PBS and fixed with PBS containing 4% paraformaldehyde for 15 min. After washing with PBS, the cells were incubated with PBS containing 3% bovine serum albumin for blocking for 1 hour at room temperature. The cells were washed three times with PBST and then incubated with an anti-ACE2 recombinant rabbit monoclonal antibody (SN0754, Invitrogen) recognizing an epitope at amino acid positions 190-230 as the primary antibody for 1 hour at room temperature. The cells were washed with PBST and then incubated with an Alexa Fluor 488-conjugated goat anti-rabbit IgG antibody (A-21206, Molecular Probes) as a secondary antibody and counterstained with 1 μg/ml 4',6-diamidino-2-phenylindole, dihydrochloride (DAPI) (D1306, Molecular Probes) for 1 hour in the dark at room temperature. Images were acquired with a 63 × oil objective lens on a Zeiss LSM700 inverted microscope using ZEN 2009 software (Carl Zeiss).

Flow cytometry

HEK293T cells were seeded in 6-well plates (2.0×10^4 cells per well) precoated with poly-L-lysine (Cultrex, R&D Systems). After 24 hours, the cells were transfected with pCAGGS encoding FLAG-tagged ACE2 WT or SNV mutant proteins using TransIT-LT1. At 24 hours post-transfection, these cells were washed with PBS and detached using 0.25% trypsin. Cells were fixed with PBS containing 4% paraformaldehyde for 15 min. After washing with PBS, cells were incubated with an anti-ACE2 recombinant rabbit monoclonal antibody (SN0754, Invitrogen) for 1 hour at room temperature. Then, the cells were stained with the Alexa Fluor 488-conjugated goat anti-rabbit IgG antibody (A-21206, Molecular Probes) for 30 min at 4°C in the dark. After washing two times, the surface expression of the exogenous ACE2 proteins was analyzed by FACSCanto flow cytometer (BD Biosciences) and FlowJo software (Tree Star).

Statistical analysis

All statistical analyses were performed using R software (Version 3.6.0). For the comparison of relative infectivities, one-way analysis of variance followed by the Dunnett test was used. *p*-values of less than 0.05 were considered statistically significant.

Results

Selection of ACE2 SNVs for the analysis

Using deep mutational scanning analyses of ACE2, amino acid substitutions that altered the binding affinity to RBD of the SARS-CoV-2 S protein were previously identified [29]. Of these, 31 substitutions coincided with the reported nonsynonymous SNV substitutions in ACE2 [30]. These studies showed that 13 SNV substitutions (S19P, I21V, I21T, E23K, A25T, K26R, T27A, E35D, N64K, E75G, T92I, Q102P, and H378R) increased the interaction with the RBD of the SARS-CoV-2 S protein, whereas 18 SNV substitutions (E35K, E37K, Y50F, N51D, N51S, M62V, K68E, F72V, M82I, G326E, E329G, G352V, D355N, Q388L, P389H, H505R, R514G, and Y515C) showed negative effects for the ACE2-RBD binding. Since the I21V/T and N51D/S mutations were shown to have similar effects on the RBD-ACE2 interaction, I21T and N51D were selected for further analyses. In total, 29 nonsynonymous SNVs were analyzed for the following experiments (Table 1). The ACE2 molecule (805 amino acids) consists of the protease domain (PD), which is known to interact with RBD of the S protein, and the collectrin-like domain (CLD), which contains the neck domain (ND), transmembrane domain (TM), and cytoplasmic tail (CT) (Fig. 1a). All 29 SNV positions were found in PD (Fig. 1b).

Table 1. Information on human ACE2 SNV mutants validated in this study

rsID[a]	Position	Amino Acid wildtype/mutant	SNV name	Binding affinity to RBD of SARS-CoV-2 S[b]
rs73635825	19	S/P	S19P	Increased
rs1244687367	21	I/T	I21T	Increased
rs756231991	23	E/K	E23K	Increased
rs1434130600	25	A/T	A25T	Increased
rs4646116	26	K/R	K26R	Increased
rs781255386	27	T/A	T27A	Increased
rs778500138	35	E/D	E35D	Increased
rs1348114695	35	E/K	E35K	Decreased
rs146676783	37	E/K	E37K	Decreased
rs1192192618	50	Y/F	Y50F	Decreased
rs760159085	51	N/D	N51D	Decreased
rs1325542104	62	M/V	M62V	Decreased
rs1199100713	64	N/K	N64K	Increased
rs755691167	68	K/E	K68E	Decreased
rs1256007252	72	F/V	F72V	Decreased
rs867318181	75	E/G	E75G	Increased
rs766996587	82	M/I	M82I	Decreased
rs763395248	92	T/I	T92I	Increased
rs1395878099	102	Q/P	Q102P	Increased
rs759579097	326	G/E	G326E	Decreased
rs143936283	329	E/G	E329G	Decreased
rs370610075	352	G/V	G352V	Decreased
rs961360700	355	D/N	D355N	Decreased
rs142984500	378	H/R	H378R	Increased
rs751572714	388	Q/L	Q388L	Decreased
rs762890235	389	P/H	P389H	Decreased
rs1016409802	505	H/R	H505R	Decreased
rs1352194082	514	R/G	R514G	Decreased
rs1263424292	515	Y/C	Y515C	Decreased

[a]NCBI ID numbers of ACE2 SNVs. [b]The effects of the substitutions on the binding affinity to the RBD of the SARS-CoV-2 S protein were obtained from previous studies [29,30].

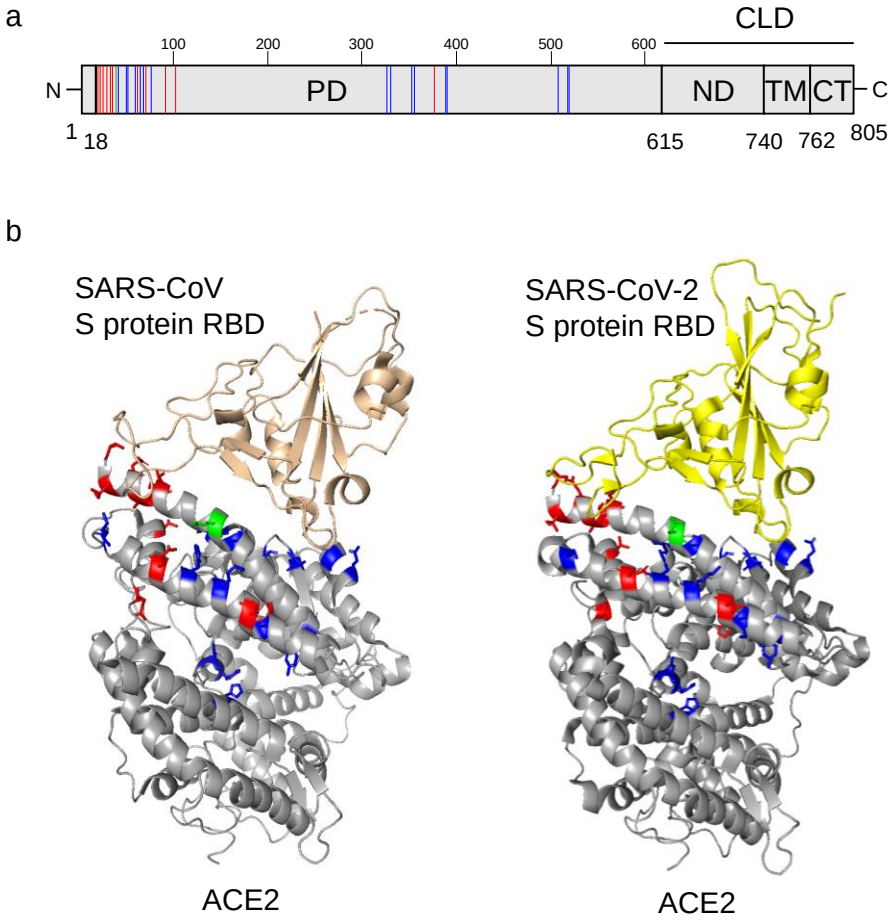

Fig. 1. Structures of ACE2 and SARS CoV S proteins

(a) Schematic diagram of human ACE2. ACE2 is a type I membrane protein, consisting of an N-terminal signal peptide, extracellular domain containing a protease domain (PD) and neck domain (ND), transmembrane domain (TM), and cytoplasmatic tail (CT). ND, TM, and CT form the collectrin-like domain (CLD). The amino acid positions of ACE2 SNVs that were reported to increase and decrease the interaction to the RBD of the SARS-CoV-2 S protein are shown as red and blue lines, respectively. The substitution at position 35 (E35D and E35K) of ACE2 showing inconsistent effects is shown as a green line. (b) Crystal structures of the complex of ACE2 and SARS CoV S proteins. The structural data were obtained from Protein Data Bank (PDB) (https://www.rcsb.org/) (PDB ID: 2AJF and 6lzg). Human ACE2, SARS-CoV RBD, and SARS-CoV-2 RBD polypeptides are shown as ribbon models in gray, pink, and yellow, respectively. The amino acid positions of ACE2 SNVs that were reported to increase and decrease the interaction to the RBD of the SARS-CoV-2 S protein are shown in red and blue, respectively. The substitution at position 35 (E35D and E35K) of ACE2 showing inconsistent effects is shown in green. The amino acid positions indicated in Fig. 1a are shown in the same colors.

ACE2 SNV substitutions that affected the cellular entry of SARS-CoV and SARS-CoV-2

To evaluate the influence of these ACE2 SNV substitutions on the cellular entry of SARS CoVs, HEK293T cells expressing exogenous ACE2 WT and SNV mutants were infected with VSIVs pseudotyped with the S proteins of SARS-CoV (VSIVΔG*-SCoV), SARS-CoV-2 (VSIVΔG*-SCoV-2), and VSIV G (VSIVΔG*-G), and the relative infectivities were compared to those of the cells expressing WT ACE2 (Fig. 2a). Although SARS-CoV and -CoV-2 entry into empty vector-transfected cells was observed at low titers, the infectious units were increased significantly by the expression of exogenous ACE2, suggesting that the entry via the alternative pathways [38] had limited impact in the comparison among the ACE2 proteins in this experimental conditions. It was found that some of the ACE2 SNV substitutions positively or negatively affected the infectivity of VSIVΔG*-SCoV and/or VSIVΔG*-SCoV-2. G352V and Y515C substitutions in ACE2 significantly enhanced the entry of VSIVΔG*-SCoV but not VSIVΔG*-SCoV-2. H505R substitution significantly enhanced the entry of both VSIVΔG*-SCoV and VSIVΔG*-SCoV-2. On the other hand, the D355N substitution significantly reduced the infectivity of VSIVΔG*-SCoV but not VSIVΔG*-SCoV-2. These results indicated that the amino acid residue at position 505 of ACE2 was commonly important for cell susceptibilities to both SARS-CoV and SARS-CoV-2, whereas the roles of the amino acid residues at positions 352, 355, and 515 in the interaction with the S protein might be different between SARS-CoV and SARS-CoV-2. As expected, none of the examined SNV substitutions significantly affected the infectivity of VSIVΔG*-G. It was confirmed that most of the ACE2 SNV mutants exogenously introduced into HEK293T cells were expressed to similar extents, except for a few mutants such as E23K and E329G that did not affect the viral infectivity (Figs. 2b and 2c). In immunofluorescence assay and flow cytometric analysis, these representative ACE2 SNV mutants (G352V, D355N, H505R, and Y515C) were similarly localized on the cell surface as was the case with WT ACE2 (Fig. 3). Taken together, these results suggested that SNV substitutions of human ACE2 affected the entry of SARS CoVs into cells.

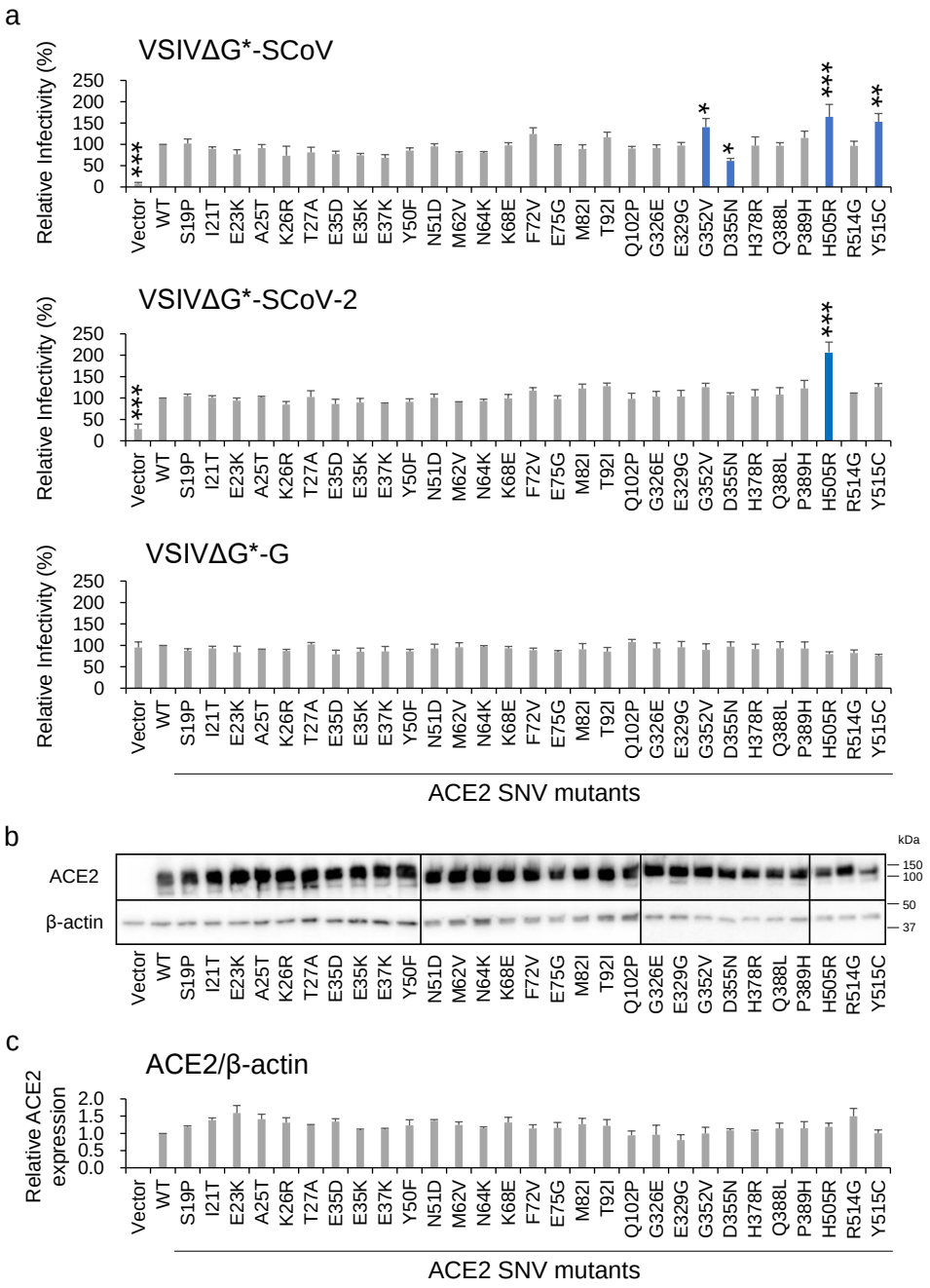

Fig. 2. Effects of ACE2 SNV substitutions on the infectivity of VSIVs pseudotyped with the S protein of SARS-CoV and SARS-CoV-2

(a) HEK293T cells transfected with the plasmids expressing WT ACE2 or its SNV mutants were infected with VSIVΔG*-SCoV, VSIVΔG*-SCoV-2, and VSIVΔG*-G. IUs were determined by counting the numbers of GFP-expressing cells at 24 hours post-infection. Relative infectivities of pseudotyped VSIVs in the cells transfected with each plasmid were determined by setting the IU value given by HEK293T cells expressing

exogenous WT ACE2 to 100%. The means and standard deviations (SDs) of three independent experiments are shown. Statistical significance was calculated compared to WT using the Dunnett test (*$p < 0.05$, **$p < 0.01$, ***$p < 0.001$). (b) HEK293T cells transfected with the plasmids expressing WT ACE2 or its SNV mutants were harvested at 48 hours post-transfection and analyzed in SDS-PAGE and Western blotting. The amounts of β-actin in the total cell lysate were also analyzed as an internal control. (c) The band intensities of WT and mutant ACE2 molecules were compared. The ratios of the expression levels of ACE2 were analyzed. The value of WT ACE2 was set to 1.0. The means and SDs of three independent experiments are shown. Statistical significance was calculated using the Dunnett test and no significant difference was detected between WT and mutant proteins.

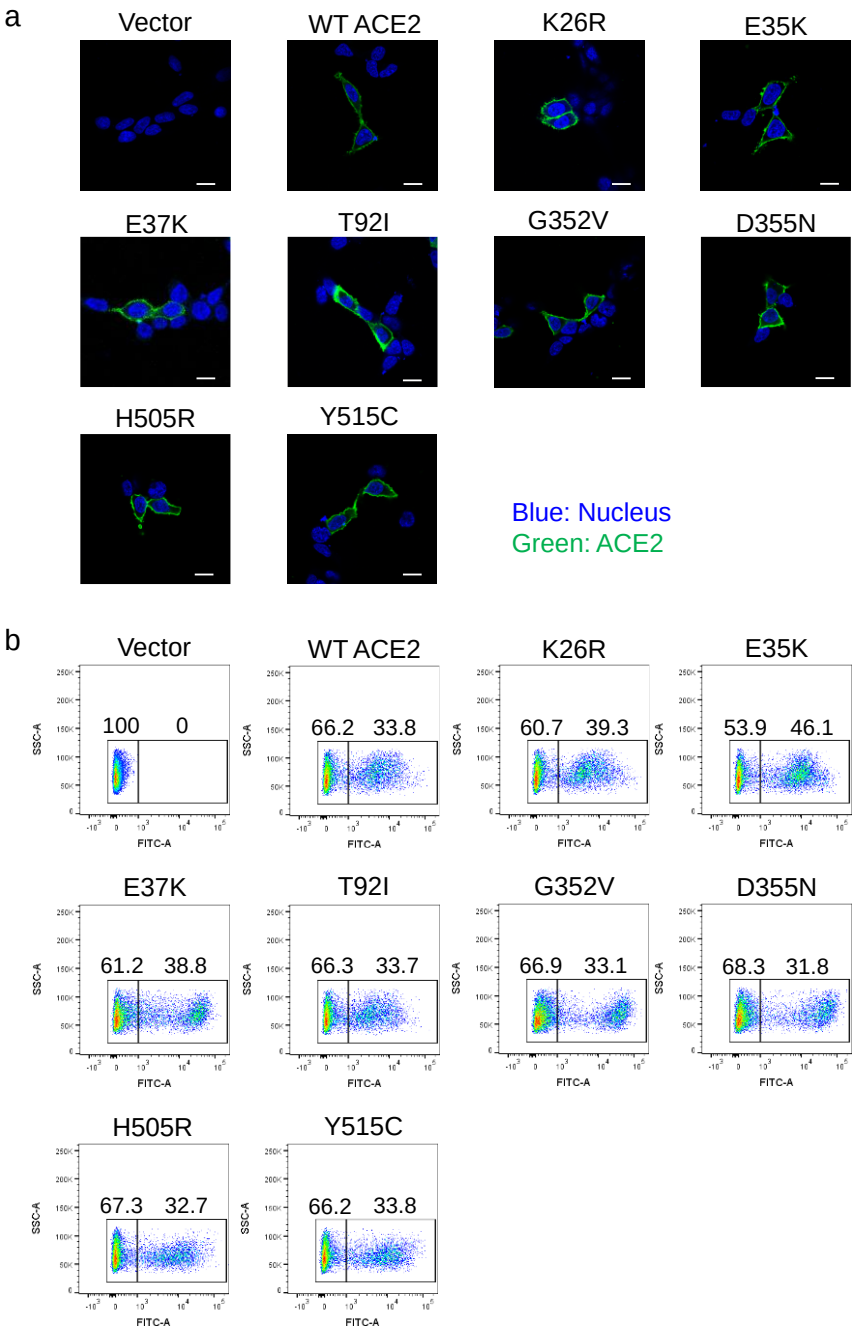

Fig. 3. Cell surface expression of ACE2 in HEK293T cells

(a) HEK293T cells transfected with the ACE2-expressing plasmids were immunostained with an anti-ACE2 monoclonal antibody and Alexa Fluor 488-conjugated goat anti-rabbit IgG and analyzed by confocal microscopy. Nuclei of cells were stained with DAPI. The scale bars represent 10 μm. (b) The surface expression of exogenously introduced ACE2 was analyzed by flow cytometry. HEK293T cells transfected with the plasmids were immunostained with the same antibodies as described above. After washing, the cells were analyzed using a FACSCanto flow cytometer.

ACE2 SNV substitutions that affected the cellular entry of SARS-CoV-2 VOCs

I next investigated whether the 29 SNVs could affect the cellular entry of VOCs (Alpha, Beta, Gamma, and Delta) of SARS-CoV-2, which had some signature substitutions in RBD of the S protein (Fig. 4). VSIVs pseudotyped with the S protein having VOC-derived substitutions in RBD of the S protein were prepared and infectivities in HEK293T cells expressing each ACE2 protein were determined. Infectivities of VSIVΔG*-SCoV-2 Alpha (N501Y) and Delta (L452R-T478K) were significantly enhanced by the H505R substitution ($p = 0.001$). The Y515C substitution also promoted the infection with SCoV-2 Delta ($p = 0.0383$). In contrast, these substitutions did not significantly affect the infectivity of VSIVΔG*-SCoV-2 Beta (K417N-E484K-N501Y) or Gamma (K417T-E484K-N501Y). Interestingly, however, infectivities of VSIVΔG*-SCoV-2 Beta and Gamma were significantly reduced by the E35K substitution ($p = 0.0266$ and 0.0125, respectively) but those of VSIVΔG*-SCoV-2 Alpha and Delta were not. Although not statistically significant compared to HEK293T expressing WT ACE2, some other ACE2 substitutions slightly affected the infection: T92I and Y515C enhanced VSIVΔG*-SCoV-2 Alpha ($p = 0.0953$ and 0.0665, respectively), K26R and E37K reduced VSIVΔG*-SCoV-2 Beta ($p = 0.059$ or 0.061), and T92I enhanced VSIVΔG*-SCoV-2 Delta ($p = 0.0557$). It was confirmed that these ACE2 SNV mutants (K26R, E35K, E37K, and T92I) were also localized on the cell surface (Fig. 3). These data suggested that effects of ACE2 SNV substitutions on SARS-CoV-2 entry into cells might be different among the SARS-CoV-2 variants.

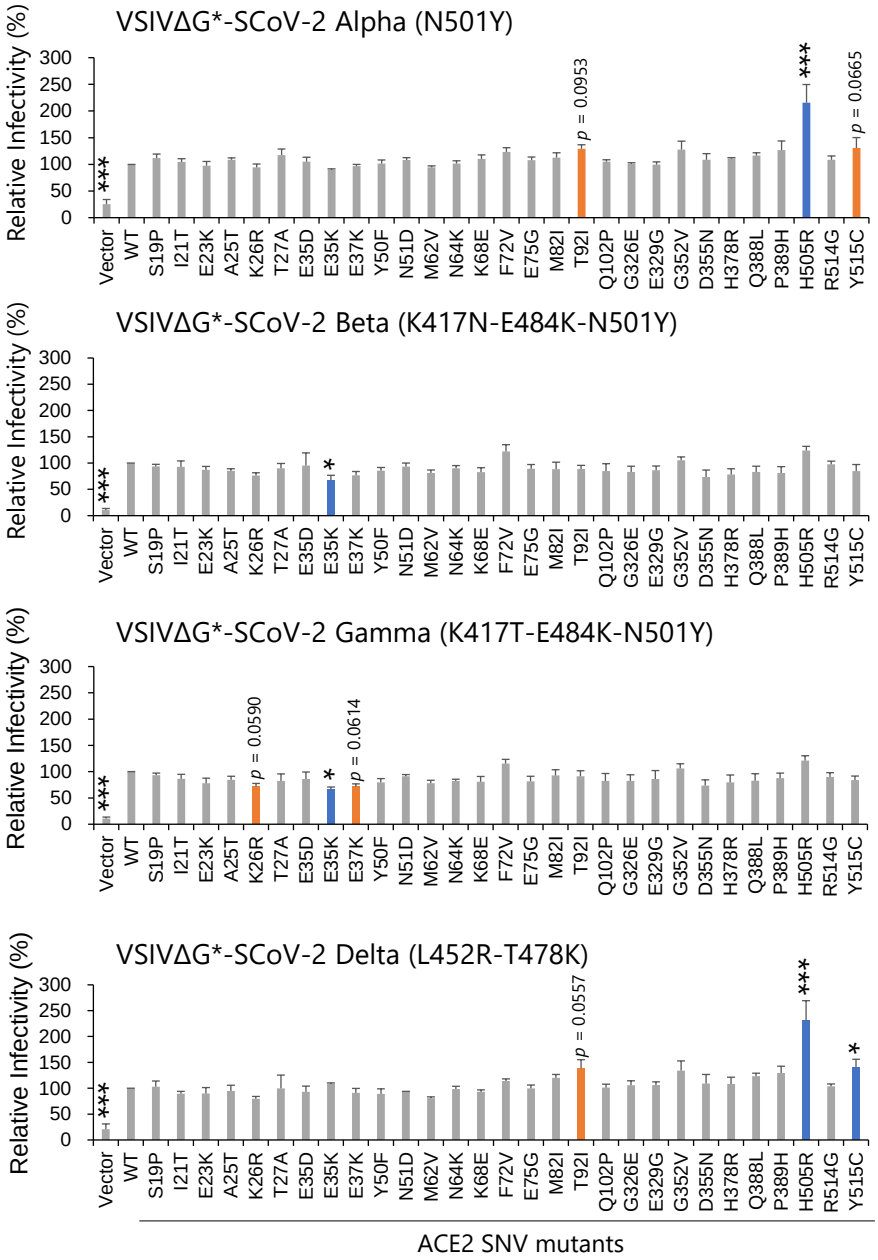

Fig. 4. Effects of ACE2 SNV substitutions on the infectivity of VSIVs pseudotyped with the S protein with VOC mutations

HEK293T cells transfected with the plasmids expressing WT ACE2 or its SNV mutants were infected with VSIVs pseudotyped with S proteins having RBD substitutions found in SARS-CoV-2 Alpha (N501Y), Beta (K417N, E484K, and N501Y), Gamma (K417T, E484K, and N501Y), and Delta (L452R and T478K) variants. Relative infectivities of pseudotyped VSIVs were determined as described in the legend of Fig. 1. The means and SDs of three independent experiments are shown. Statistical significance was calculated compared to WT using the Dunnett test (*$p < 0.05$, ***$p < 0.001$).

Molecular position and allele frequencies of the selected ACE2 SNV mutants

Five SNV substitutions in ACE2 (E35K, G352V, D355N, H505R, and Y515C) was found to significantly affect the cellular entry of SARS CoVs. E35K, G352V, and D355N were involved in the interaction site with the S protein whereas H505R and Y515C were located far from the interaction site (Fig. 5a). Using public SNP databases, TOPMed, genomAD, and ExAC, the allele frequencies of these mutants were compared (Table 2). E35K, G352V, D355N, H505R, and Y515C are uncommon in the global population (minor allele frequency [MAF] = 0.00001, 0.00003, 0.00001, 0.00001, and 0.000004, respectively). E35K is more frequently found in the East Asian population (MAF = 0.0001) when compared with the global population. Thus, the allele frequencies of the SNV mutants that could potentially alter the cell susceptibility to SARS CoVs was found to be very low in the current population.

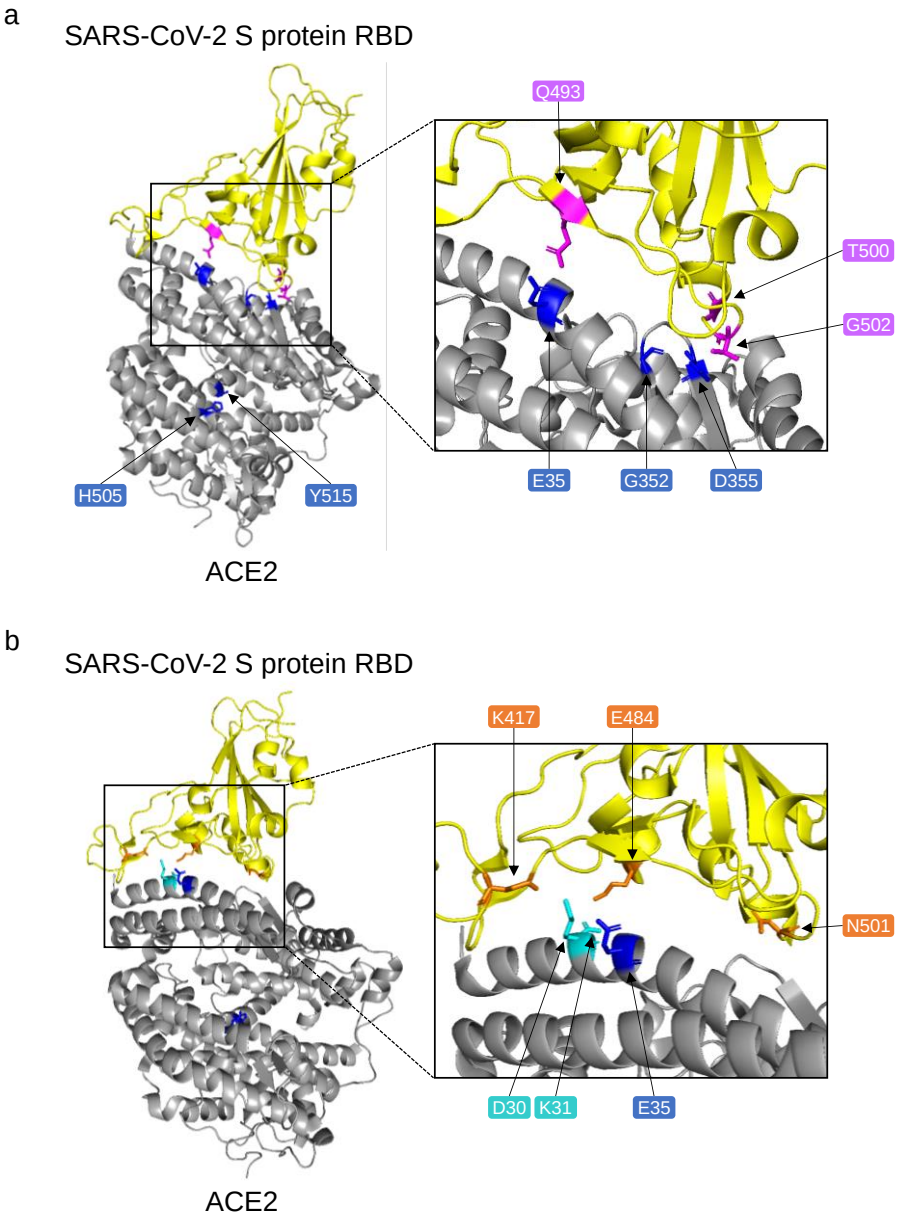

Fig. 5. Amino acid positions of the ACE2 SNV substitutions that affected the cellular entry of SARS-CoV and SARS-CoV-2

The crystal structure of the complex of ACE2 and the SARS-CoV-2 S protein (PDB ID: 6lzg). The amino acid positions of five ACE2 SNVs that affected the cellular entry of SARS-CoV and/or SARS-CoV-2 are shown in blue. (a) Two amino acid residues (T500 and G502) and Q493 in the S protein of SARS-CoV-2, which are shown in magenta, are known to bind to D355 and E35 of ACE2, respectively. (b) Three amino acid positions (K417, E484, and N501) at which substitutions were found in the S protein of SARS-CoV-2 Beta and Gamma variants are shown in orange. K417 and E484 in the S protein, which are known to bind to D30 and K31 of ACE2, respectively, are shown in cyan.

Table 2. Minor allele frequencies of human ACE2 SNV substitutions that affected the entry of SARS CoVs

SNVs	Minor allele frequencies[a]					
	Global	African	American	East Asian	South Asian	European
E35K	0.00001	0	0	0.0001	0	0.00001
G352V	0.00003	0	0	0	0	0.00007
D355N	0.00001	0	0	0	0	0.00002
H505R	0.00001	NA[b]	NA	NA	NA	NA
Y515C	0.000004	NA	NA	NA	NA	NA

[a]Minor allele frequencies of ACE2 SNVs among different populations were obtained from TOPMed, ExAC, or gnomAD. [b]NA: Information are not available in the databases.

Discussion

While ACE2 acts as a receptor for SARS CoVs, human ACE2 SNVs have been reported to be associated with cardiovascular diseases, hypertension, and diabetic mellitus, all of which are recognized as risk factors for severe clinical outcomes in COVID-19 patients [39–41]. Genetic variations in the host ACE2 receptor may also influence the susceptibility or resistance to the SARS-CoVs. Several *in silico* studies suggested that ACE2 SNVs might affect the binding affinity to the S protein [27,42,43]. However, only a few studies have reported on the biological importance of ACE2 SNVs in the cellular entry of SARS-CoVs [18,28,44], and the information on this topic is still limited. Previous studies demonstrated that some ACE2 SNV substitutions affected the binding affinity to RBD of the SARS-CoV-2 S protein [29,30]. In the present study, I investigated the effects of these SNV substitutions on actual viral entry into cells using pseudotyped VSIVs.

It was found that the G352V substitution significantly enhanced the entry of SARS-CoV but affected that of SARS-CoV-2 only slightly. In contrast, the D355N substitution significantly reduced the entry of SARS-CoV but not SARS-CoV-2. Since the amino acid residue at position 352 in ACE2 is adjacent to a loop structure that is responsible for the interaction with the S proteins of SARS CoVs [45,46], the G352V substitution likely affects the structure and/or molecular flexibility of this loop, which might result in enhanced binding to the S protein. Cryo-electron microscopy (cryo-EM) of the structures of the ACE2 and S protein complexes revealed that the aspartic acid at position 355 of human ACE2 formed hydrogen bonds and van der Waals contacts with 3 (T486, T487, and G488) and 2 (T500 and G502) amino acid residues of SARS-CoV and SARS-CoV-2 S proteins, respectively [47]. Differences in the number of van der Waals contacts might contribute to the differential effects of the D355N substitution between SARS-CoV and SARS-CoV-2. In another cocrystal structure of the SARS-CoV-2 S protein and ACE2, 22 residues in the ACE2 molecule are involved in the binding to the S protein of SARS-CoV-2 [47] and 6 of the 22 amino acid positions were reported to be SNV positions (S19P, T27A, E35D/K, E37K, M82I, and D355N). Another group demonstrated that the binding affinity to RBD of the SARS-CoV-2 S protein was increased in S19P, T27A, and E35D mutants and was reduced in E35K, E37K, M82I, and D355N mutants [48]. However, these SNV substitutions, except E35K, did not significantly affect the viral infectivity in the present study (Figs. 2 and 4). Since a recombinant RBD molecule lacking all the other portions of the S protein was used in the previous binding assays [29,48] one possible explanation is that structural and functional differences between the RBD molecule and the full-length whole S protein might affect the affinity or avidity to ACE2. Furthermore,

cryo-EM analyses revealed that the SARS-CoV-2 S protein had RBD-exposed conformation (open) and RBD-buried conformation (closed) and a high proportion of the S protein showed closed conformation [49,50], which might weaken the effects of the substitutions in ACE2 when the whole S protein molecule is used for analyses. This difference between RBD and full-length S protein molecules could be one of the reasons for the lesser effects of the ACE2 substitutions on the SARS-CoV 2 entry than on the RBD binding capacity to ACE2.

The H505R substitution in ACE2 enhanced the entry of both SARS-CoV and SARS-CoV-2, including some VOCs. The Y515C substitution also tended to enhance the entry. These residues are not directly involved in the molecular surface that interacts with RBD of the S protein. The histidine residue at position 505 of ACE2 is thought to be a catalytic histidine based on a site-directed mutagenesis experiment for the ACE2 enzymatic activity [51]. Furthermore, this amino acid residue may be important for the hydrogen bond to the tyrosine at position 515, which has been suggested to stabilize the carbonyl tetrahedral intermediate in the ACE2 molecule [51,52]. Thus, these SNV mutants might have altered enzymatic activities, while the structure of ACE2 might also be affected by the substitutions. However, a previous study reported that the ACE2 binding region of the SARS-CoV S protein was not interfered with inhibitors or substrates that induced large conformational changes in the receptor, suggesting that the enzymatic activity of ACE2 does not contribute to SARS-CoV S protein-mediated infection [53].

In the immunoblotting image (Fig. 2b), two bands were detected, which corresponded to unglycosylated (85-90 kD) and glycosylated (110-120 kD) forms of the ACE2 protein. N-glycosylation is required for proper ACE2 expression on the cell surface and efficient viral entry of SARS-CoV-2 [54]. The ACE2 molecule has seven N-glycosylation sites (N53, N90, N103, N322, N432, N546, and N690) and a molecular dynamics simulation study reported that two glycosylation sites, N90 and N322, affected the binding capacity to the SARS-CoV-2 S protein [55]. Another study showed that the mutation at T92 removing the N90-glycosylation motif enhanced the interaction with the S protein of SARS-CoV-2 [29]. However, since the amino acid positions assessed in this study were not located in the reported N-glycosylation sites except for T92I and the majority of the detected bands were most likely glycosylated forms, N-glycosylation patterns might not affect the cell surface expression and binding efficiency of ACE2.

It was previously demonstrated that the H505R and Y515C ACE2 mutants showed weak binding affinity to RBD of the SARS-CoV-2 S protein [30]. This discrepancy may also be due to the structural difference between RBD and full-length S protein molecules as discussed above. Alternatively, it may also be possible that weak binding capacity of

ACE2 mutants does not necessarily cause reduced entry of the virus. A previous molecular dynamics analysis suggests that the ACE2 structural changes caused by some SNV substitutions likely affect the stability of the ACE2 molecule [56], which may influence the efficiency of membrane fusion. I speculate that H505R and Y515C mutants may have enhanced potential to support membrane fusion, which overwhelms their reduced binding to the S protein and results in increased entry of the virus.

Interestingly, the E35K substitution reduced the entry of SARS-CoV-2 variants with triple substitutions in their RBD (i.e., Beta and Gamma) but not the other viruses tested, including the Alpha variant, which also had N501Y substitution, suggesting that the effect of the E35K substitution might be related to the K417N and/or E484K substitutions commonly found in Beta and Gamma variants. It has been shown that the lysine residue at position 417 forms a salt bridge with the aspartic acid at position 30 of ACE2, and the glutamic acid at position 484 interacts with the lysine at position 31 of ACE2 (Fig. 5b) [47,57]. The importance of the lysine at 417 and the glutamic acid at 484 for the interaction with ACE2 suggests the possibility that K417N and E484K substitutions negatively affect the binding to the ACE2 E35K mutant. Another study showed that the triple substitution (K417N, E484K, and N501Y) in the Beta variant changed the secondary structure and stability of RBD of the SARS-CoV-2 S protein [58]. Taken together, the structural changes caused by these substitutions in RBD of the S protein might reduce the interaction with the ACE2 E35K mutant.

Genetic polymorphisms of the ACE2 and TMPRSS2 genes have been suggested to be involved in the disease outcomes of SARS-CoV-2 infection [22]. The present data support the notion that ACE2 SNVs may contribute to the enhancement or reduction of cell susceptibility to SARS CoVs, although the SNV substitutions that were found to be important in this study are rare in the current human population. It should also be noted that the effects of ACE2 SNVs cannot be determined solely from RBD binding assays, as demonstrated by the inconsistent results between previous RBD binding assays and viral entry assays in the present study. The limitation of the present study is that I only focused on the single step of viral entry and the effects of ACE2 SNV substitutions were not very drastic; however it is assumed that the differences among ACE2 variants may be enhanced in multiple replication cycles of authentic SARS-CoV and SARS-CoV-2. Furthermore, it still needs to be clarified whether ACE2 SNVs affect the clinical outcomes in COVID-19 patients. In the future, large-scale clinical studies of genetic variations are needed to confirm the significance of SNVs *in vivo* and to further understand possible relationships between host genetic factors and SARS-CoV-2 evolution.

Summary

SARS-CoV and SARS-CoV-2 have a single envelope glycoprotein (S protein) that binds to human ACE2 on the host cell membrane. Previous mutational scanning studies have suggested that some substitutions corresponding to SNVs in human ACE2 affect the binding affinity to the RBD of the SARS-CoV-2 S protein. However, the importance of these substitutions in actual virus infection is still unclear. In this study, the effects of the reported ACE2 SNV substitutions on the entry of SARS-CoV and SARS-CoV-2 into cells were investigated, using VSIV pseudotyped with S proteins of these CoVs. HEK293T cells transfected with plasmids expressing ACE2 having each SNV substitution were infected with the pseudotyped VSIVs and relative infectivities were determined compared to the cells expressing WT ACE2. It was found that some of the SNV substitutions positively or negatively affected the infectivities of the pseudotyped viruses. Particularly, the H505R substitution significantly enhanced the infection with the pseudotyped VSIVs, including those having the substitutions found in the S protein RBD of SARS-CoV-2 variants of concern. These results suggest that human ACE2 SNVs may potentially affect cell susceptibilities to SARS-CoV and SARS-CoV-2.

Chapter II

Single nucleotide variants of the human TIM-1 IgV domain with reduced ability to promote viral entry into cells

Introduction

The members of the T-cell immunoglobulin mucin (TIM) family are type I transmembrane glycoproteins [59]. Of these, TIM-1 is expressed on various immune cells and a broad range of mucosal epithelial cells and plays roles in regulating immune responses, allergic responses, asthma, and transplant tolerance [60–63]. One of the physiological functions of TIM-1 is to recognize phosphatidylserine (PS) exposed on the apoptotic cell surface and mediate phagocytosis of those cells [64]. PS receptors such as TIM-1 are also known to recognize PS exposed on the viral envelope, and TIM-1 promotes viral entry into host cells through interactions with viral envelope-associated PS, which is known as "the viral apoptotic mimicry strategy" [65]. Mainly through this mechanism, TIM-1 is known to enhance the cellular entry of a wide range of enveloped viruses, including filovirus, flavivirus, alphavirus, arenavirus, rhabdovirus, and baculovirus [13,66]. In addition, previous studies demonstrated that the virus−TIM-1 interaction induced a release of inflammatory cytokines from primary $CD4^+$ T cells and might also contribute to the pathogenesis of Ebola virus (EBOV) infection in mice [67,68]. TIM-1 was shown to activate dengue virus-induced autophagy through the TIM-1 signaling pathway [69]. Therefore, TIM-1 is thought to play an important role not only as a viral attachment receptor but also as an immune-regulatory molecule against some viruses.

TIM-1 is composed of an immunoglobulin variable (IgV) domain, mucin-like domain (MLD), transmembrane domain, and cytoplasmic tail (CT) (Fig. 6a). The IgV domain is essential for the TIM-1-mediated enhancement of viral infections, and MLD is thought to be necessary to place the IgV domain within the appropriate distance from the cell surface [70,71]. Previous studies reported that genetic polymorphisms of human TIM-1 (hTIM-1) MLD and IgV domain affected its function to promote viral infections. A polymorphism with a six amino acid insertion into hTIM-1 MLD was associated with reduced and enhanced disease progression with human immunodeficiency virus and hepatitis A virus infection, respectively [72,73]. It was also reported that this insertion influenced *in vitro* cell susceptibility to Japanese encephalitis virus [74]. A single nucleotide variant (SNV), the S51L variant (NCBI ID: rs2270922), of the hTIM-1 IgV

domain was reported to have reduced ability for the hTIM-1-mediated entry of pseudotyped lentivirus with chikungunya virus GP [75]. In addition, a previous study showed that a polymorphism of the TIM-1 IgV domain among African green monkey cell lines affected the efficiency of the cellular entry of VSIV pseudotyped with EBOV GP [76]. From these findings, I hypothesized that SNVs of the hTIM-1 IgV domain might influence cell susceptibilities to viral infections. However, there are few studies focusing on the effects of SNVs of the TIM-1 IgV domain on viral entry into cells, and the information supporting this hypothesis is still limited.

The crystal structure of the IgV domain revealed that this domain has two antiparallel β sheets: a "BED-β sheet" consisting of β-strands B, E, and D and a "GFC-β sheet" consisting of β-strands A, G, F, C, C', and C" [77]. Three loops between β-strands B and C, C and C', and F and G are named the BC loop, CC' loop, and FG loop, respectively (Figs 6b and 6c). Six cysteine residues (C36, C46, C52, C57, C104, and C105) in the IgV domain form disulfide bonds on the GFC β-sheet. Two cysteine residues, C36 and C105, form a disulfide bond (C36-C105) between β-strand F and the BC loop, and four cysteine residues (C46, C52, C57, and C104) form two additional disulfide bonds (C46-C57 and C52-C104) that fix the CC' loop onto the GFC β-sheet [78,79]. These bonds define a cleft formed by the CC' and FG loops, providing a unique groove-like structure to bind PS, identified as the "PS-binding pocket" (Fig. 1c). This structure is conserved among the TIM family and is also called the metal-ion-dependent ligand binding site (MILIBS), which was identified as an important region for binding to viral PS [78]. It has also been shown that the three loops (BC, CC', and FG loops) of the IgV domain interact with both the EBOV GP and PS exposed on the viral envelope [80]. These findings led me to hypothesize that SNV substitutions in the IgV domain might affect the function of hTIM-1 to promote viral entry into cells.

In this chapter, the potential effects of hTIM-1 SNV substitutions on cellular entry of enveloped viruses were evaluated using pseudotyped VSIVs. I focused on SNVs of the IgV domain as a key part for binding to virus particles and found 35 missense SNVs in the public gene database (Ensembl genome browser). Of these, some SNV substitutions reduced the efficiency of hTIM-1-mediated cellular entry of VSIVs having GPs of different origins. The present study suggests that some SNVs of the hTIM-1 IgV domain may have a lower ability to bind PS and/or viral GPs on pseudotyped VSIV particles.

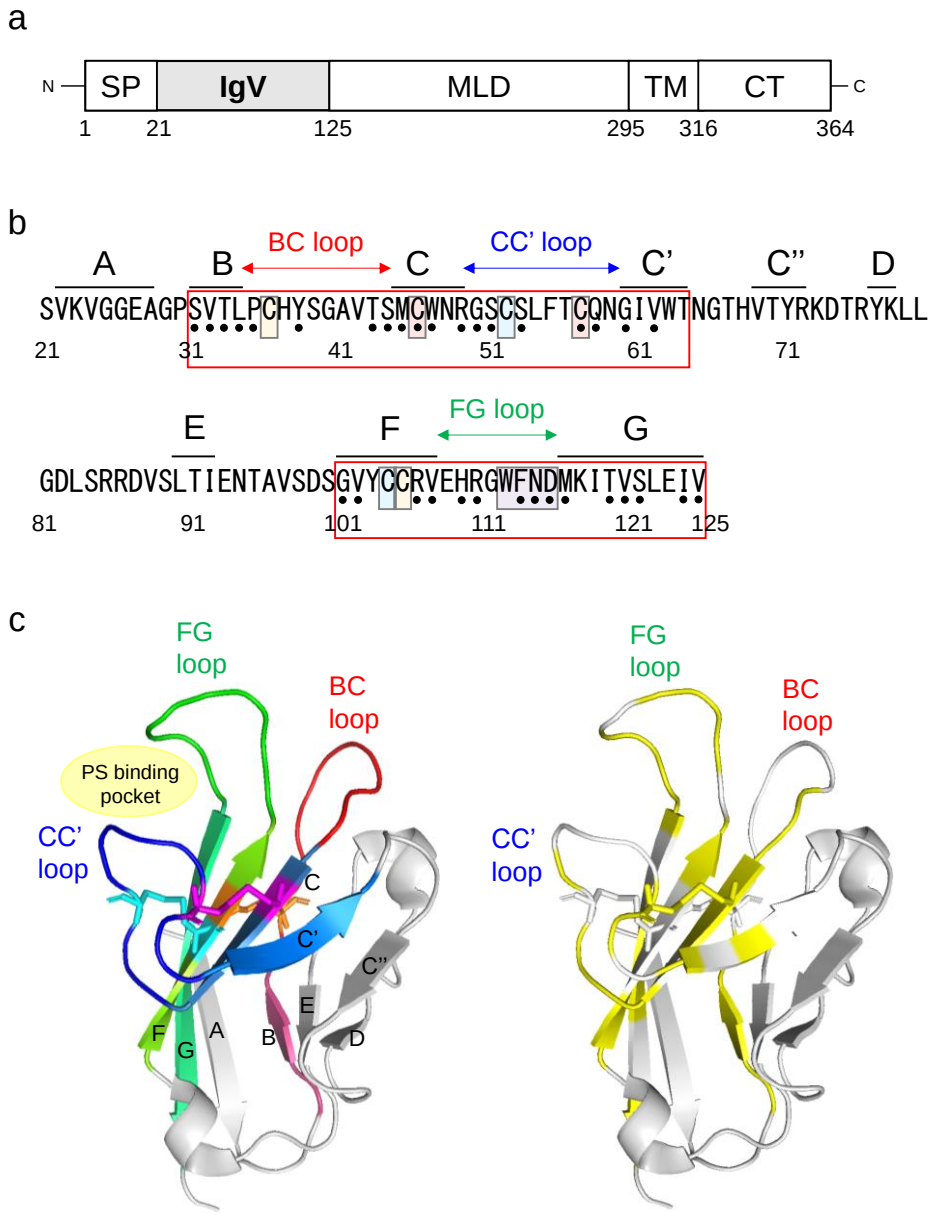

Fig. 6. Structure of the hTIM-1 IgV domain and the 35 SNV substitutions examined in this study

(a) Schematic diagram of hTIM-1. TIM-1 consists of a signal peptide (SP), immunoglobulin variable (IgV) domain, mucin-like domain (MLD), transmembrane domain (TM), and cytoplasmic tail (CT). (b) Amino acid sequence of the hTIM-1 IgV domain (positions 21-125; GenBank accession number: NM_012206.3). Regions corresponding to each β-strand are shown above the sequence. Six cysteine residues forming three disulfide bonds (C36-C105, C46-C57, and C52-C104) are highlighted in orange, magenta, and cyan pairs, respectively. The PS-binding site (WFND motif) is highlighted in purple. Black dots under the sequence indicate the 35 SNV positions

examined in this study. (c) Crystal structure of the hTIM-1 IgV domain (PDB ID: 5DZO). In the left panel, β-sheets are labeled with their corresponding β-strand names, and five β-strands, B, C, C', F, and G, are colored in warmpink, skyblue, marine, chartreuse, and limegreen, respectively. BC, CC', and FG loops are colored in red, blue, and green, respectively. Amino acid residues involved in three disulfide bonds (C36-C105, C46-C57, and C52-C104) are shown in orange, magenta, and cyan, respectively. In the right panel, the 35 SNV positions are shown in yellow.

Materials and Methods

SNV information on the hTIM-1 IgV domain

Nucleotide sequences of the hTIM-1 IgV domain were obtained from the Ensembl genome browser [81] and the dbSNP on the NCBI website [82], and 35 missense SNVs were found in the IgV domain. The NCBI ID numbers of these SNVs are as follows: rs774628607 (S31F), rs766684661 (V32F), rs763305471 (T33A), rs748542797 (L34P), rs1235087840 (P35S), rs948562287 (Y38H), rs1331131690 (T43A), rs1392286629 (S44P), rs201914430 (M45V), rs778524415 (C46W), rs368474218 (W47R), rs1334308674 (R49S), rs1467830805 (G50S), rs2270922 (S51L), rs766596791 (S53F), rs750683624 (C57S), rs1324375875 (Q58R), rs765450007 (G60D), s776921169 (V62I), rs1313131093 (G101D), rs759044943 (V102L), rs770585374 (R106H), rs748923252 (V107I), rs769720430 (H109P), rs370980439 (R110C), rs1196575610 (G111R), rs1240319173 (F113L), rs377678930 (N114S), rs1168125347 (D115G), rs745941787 (M116L), rs778900665 (T119I), rs754029647 (V120I), rs1190295106 (S121P), rs1169032336 (I124T), rs556857102 (V125L) (Table 3). In the present study, the most common genotype of hTIM-1 in the global population was defined as WT (GenBank accession number, NM_012206.3) based on the genetic information from NCBI.

Allele frequencies of hTIM-1 SNVs were obtained from the genomAD and TOPMed. The potential detrimental effects of hTIM-1 SNV substitutions on its structure and function were assessed by sorting intolerant from tolerant (SIFT), polymorphism phenotyping 2 (PolyPhen-2), combined annotation dependent depletion (CADD), and rare exome variant ensemble learner (REVEL). The SIFT scores are classified as tolerated (T) ($\geq$ 0.05) or deleterious (D) ($<$ 0.05). PolyPhen-2 scores are classified as benign (B) ($<$ 0.5), possibly damaging (PosD) (0.5-0.9), or probably damaging (ProD) ($\geq$ 0.9). CADD scores are classified as likely benign (LB) ($<$ 20) or likely deleterious (LD) ($\geq$ 20). REVEL scores are classified as likely benign (LB) ($<$ 0.5) or likely disease-causing (LDC) ($\geq$ 0.5). The scoring methods were taken from the following Ensemble genome browser [83].

Table 3. Thirty-five SNVs of hTIM-1 IgV domain listed in the public database

rsID[a]	Position	Amino Acid wildtype/mutant	SNV name	Location[b]
rs774628607	31	S/F	S31F	β-strand B
rs766684661	32	V/F	V32F	β-strand B
rs763305471	33	T/A	T33A	β-strand B
rs748542797	34	L/P	L34P	β-strand B
rs1235087840	35	P/S	P35S	BC loop
rs948562287	38	Y/H	Y38H	BC loop
rs1331131690	43	T/A	T43A	BC loop
rs1392286629	44	S/P	S44P	BC loop
rs201914430	45	M/V	M45V	β-strand C
rs778524415	46	C/W	C46W	β-strand C
rs368474218	47	W/R	W47R	β-strand C
rs1334308674	49	R/S	R49S	β-strand C
rs1467830805	50	G/S	G50S	CC' loop
rs2270922	51	S/L	S51L	CC' loop
rs766596791	53	S/F	S53F	CC' loop
rs750683624	57	C/S	C57S	CC' loop
rs1324375875	58	Q/R	Q58R	CC' loop
rs765450007	60	G/D	G60D	β-strand C'
s776921169	62	V/I	V62I	β-strand C'
rs1313131093	101	G/D	G101D	β-strand F
rs759044943	102	V/L	V102L	β-strand F
rs770585374	106	R/H	R106H	β-strand F
rs748923252	107	V/I	V107I	β-strand F
rs769720430	109	H/P	H109P	FG loop
rs370980439	110	R/C	R110C	FG loop
rs1196575610	111	G/R	G111R	FG loop
rs1240319173	113	F/L	F113L	FG loop
rs377678930	114	N/S	N114S	FG loop
rs1168125347	115	D/G	D115G	FG loop
rs745941787	116	M/L	M116L	β-strand G
rs778900665	119	T/I	T119I	β-strand G
rs754029647	120	V/I	V120I	β-strand G
rs1190295106	121	S/P	S121P	β-strand G
rs1169032336	124	I/T	I124T	β-strand G
rs556857102	125	V/L	V125L	β-strand G

[a]NCBI ID numbers of hTIM-1 SNVs. [b]The amino acid positions were identified from a crystal structure of the hTIM-1 IgV domain.

Cells

Human adenocarcinoma-derived alveolar basal epithelial A549, human embryonic kidney 293T, and African green monkey kidney epithelial Vero E6 cells were grown in DMEM (Sigma-Aldrich) supplemented with 10% FCS (Sigma-Aldrich), 100 U/ml penicillin, and 0.1 mg/ml streptomycin (Gibco) at 37°C in a 5% CO_2 incubator. Expi 293F cells (Gibco) were maintained in Expi 293F Expression Medium (Thermo Fisher Scientific) as described in the manufacturer's instructions and incubated at 37°C in an 8% CO_2 incubator while shaking at 125 rpm.

hTIM-1 plasmids

Total RNA was extracted from A549 cells using Trizol (Invitrogen), and then a cDNA library was prepared with SuperScript™ IV (Invitrogen) and the oligo dT20 primer (5'-TTTTTTTTTTTTTTTTTTTT-3'). To amplify the coding region of the hTIM-1 gene, PCR was performed with a KOD One polymerase (TOYOBO) using the primers EcoRI-hTIM-1-F (5'-ATAGAATTCGCCACCATGCATCCTCAAGTG-3') containing an EcoRI restriction site and XhoI-hTIM-1-R (5'-TATCTCGAGCTATTATTCCAAGCGGCTTCG-3') containing an XhoI restriction site. After sequence confirmation of the WT hTIM-1 gene, this PCR product was inserted into an expression plasmid, pCAGGS. Using this plasmid as a template, a plasmid encoding 6 × histidine-tagged WT soluble hTIM-1 (aa 1-295) was generated by PCR-based mutagenesis. SNV substitutions were produced by site-directed mutagenesis using a KOD One polymerase (TOYOBO) with primers containing the desired nucleotide substitutions. All mutations were confirmed by Sanger sequencing of the plasmids. Generation of the recombinant plasmids and proteins was approved by Hokkaido University Safety Committee for Genetic Recombination Experiments (21[4]).

Generation of pseudotyped VSIVs

Filovirus and arenavirus GPs were used in the present study. Ebola virus (EBOV), Marburg virus (MARV), and Lloviu virus (LLOV) were selected from 3 filovirus genera, Ebolavirus, Marburgvirus, and Cuevavirus, respectively [84]. Two arenaviruses, Junin virus (JUNV) and Lassa virus (LASV), were selected as representatives of the New World and Old World arenaviruses, respectively [85]. The GPs of these enveloped viruses are the only proteins that are responsible for virus entry into host cells [29]. Using replication-incompetent VSIV containing the GFP gene instead of the VSIV G gene (VSIVΔG*-VSIV), VSIVs bearing GPs of EBOV (Mayinga), MARV (Angola), LLOV (Asturias), JUNV (Candid #1), and LASV (Josiah) were generated as described previously [30], and

designated VSIVΔG*-EBOV, -MARV, -LLOV, -JUNV, and -LASV, respectively. Briefly, HEK293T cells were transfected with the pCAGGS plasmid encoding each viral GP gene. After 24-hour incubation, the culture medium was removed and the cells were incubated with VSIVΔG*-VSIV at a multiplicity of infection of 2.0 for 60 min at 37°C. After the inoculum was removed and the cells were washed 3 times with DMEM, the medium was replaced with fresh DMEM with 10% FCS. Sixteen hours later, the culture supernatants were harvested and stored at −80°C until use. Virus IUs in HEK293T cells were determined by counting the number of GFP-positive cells with an IN Cell Analyzer 2500HS (GE Healthcare). Previous studies reported that hTIM-1 enhanced the infectivities of envelope viruses including VSIV, and viral attachment through the TIM-1-PS interaction has been proposed as one of the general mechanisms for the first step of viral entry into cells [65]. In addition, the TIM-1-PS interaction was shown to be important for the infectivities of pseudotyped VSIVs by the competition assay with PS liposomes, and the presence of PS on the VSIV envelope was demonstrated in the binding assay using Annexin V [71]. Generation of the recombinant plasmids was approved by the Ministry of Education, Culture, Sports, Science, and Technology, Japan. The use of VSIVs was approved by the Committee for Safety Management of Pathogens, Research Center for Zoonosis Control, Hokkaido University (10[06]) and Hokkaido University Safety Committee for Genetic Recombination Experiments (21[4]).

Virus entry assay

HEK293T cells lacking endogenous expression of hTIM-1 [63] were seeded in 96-well plates (1.0×10^4 cells per well) precoated with poly-L-lysine (Cultrex, R&D Systems). Twenty-four hours later, the cells were transfected with 0.2 μg/well of pCAGGS encoding WT hTIM-1, its SNV mutants, or an empty plasmid as a negative control. At 24 hours post-transfection, these cells were infected with VSIVΔG*-EBOV, -MARV, -LLOV, -JUNV, -LASV, or -VSIV. Each virus was appropriately diluted to provide 200-500 IUs/well in HEK293T cells and then incubated with an anti-VSIV G monoclonal antibody (VSIV-G (N) 1-9) for 30 min at 37°C to abolish the background infectivity of parental VSIVΔG*-VSIV (i.e., inoculum virus) [32]. Twenty-four hours later, IUs were determined by counting the numbers of GFP-expressing cells using an IN Cell Analyzer 2500HS (GE Healthcare). The relative infectivity was determined by setting the IU value of empty plasmid-transfected cells to 100%.

SDS-PAGE and Western blotting

HEK293T were seeded in 24-well plates (1.0×10^4 cells per well) precoated with

poly-L-Lysine (Cultrex, R&D Systems). After overnight culture, the cells were transfected with the plasmids encoding WT hTIM-1, its SNV mutants, or the empty plasmid as a negative control. After 48-hour incubation, these cells were washed with PBS 3 times and lysed with a RIPA buffer (0.25 mM EDTA, pH 8.0, 25 mM Tris/HCl, pH 7.6, 150 mM NaCl, 1% NP-40, 1% sodium deoxycholate, 0.1% SDS). After centrifugation, the supernatants were mixed with SDS-PAGE sample buffer (Bio-Rad) with 5% 2-mercaptoethanol and subjected to 10% SDS-PAGE. Separated proteins were blotted on a polyvinylidene difluoride membrane (Merck Millipore Corporation). After blocking with 5% skim milk, the membrane was incubated with a goat anti-hTIM-1 polyclonal antibody (AF1750, R&D Systems) and anti-β-actin mouse monoclonal antibody (AC15, Abcam) as primary antibodies for 1 hour, respectively. After washing with PBST, the membrane was incubated with a HRP-conjugated donkey anti-goat IgG polyclonal antibody (705-035-003, Jackson ImmunoResearch) and goat anti-mouse IgG polyclonal antibody (115-035-062, Jackson ImmunoResearch) as secondary antibodies for 1 hour, respectively. After washing with PBST, the bound antibodies were visualized with Immobilon Western (Merck Millipore Corporation). The relative expression levels (i.e., the band intensities of hTIM-1 molecules divided by those of β-actin) were analyzed using an Amersham Imager 600 (GE Healthcare).

Immunofluorescence assay

HEK293T cells were seeded in a μ-Slide 8 Well Chamber Slide-well (iBidi GmbH) after precoating with poly-L-Lysine (Cultrex, R&D Systems). After overnight culture, the cells were transfected with the plasmids encoding WT hTIM-1 or its SNV mutant genes. At 24 hours post-transfection, the cells were washed with PBS and fixed with 4% paraformaldehyde in PBS for 15 min. After washing with PBS, the cells were incubated with PBS containing 3% bovine serum albumin for blocking for 1 hour at room temperature. After washing 3 times with PBST, the cells were incubated with a goat anti-hTIM-1 polyclonal antibody (AF1750, R&D Systems) as the primary antibody for 1 hour at room temperature. The cells were washed 3 times with PBST and then incubated with a donkey anti-goat IgG polyclonal antibody conjugated with fluorescein isothiocyanate (FITC) (sc2024, Santa Cruz Biotechnology) as a secondary antibody, followed by counterstaining with 1 μg/ml DAPI (D1306, Molecular Probes) for 1 hour in the dark at 4°C. Images were acquired with a 63 × oil objective lens on a Zeiss LSM700 inverted microscope using ZEN 2009 software (Carl Zeiss).

Flow cytometry

HEK293T cells were seeded in 6-well plates (2.5×10^4 cells per well) precoated with poly-L-lysine (Cultrex, R&D Systems) and incubated overnight at 37˚C. The cells were transfected with pCAGGS encoding WT hTIM-1 or its SNV mutant genes. At 24 hours post-transfection, the cells were washed with PBS, detached by treatment with 0.25% trypsin, and then fixed with 4% paraformaldehyde in PBS for 15 min. After washing with PBS, the cells were incubated with a goat anti-hTIM-1 polyclonal antibody (AF1750, R&D Systems) for 1 hour at room temperature. Then the cells were washed with PBST and stained with a donkey anti-goat IgG polyclonal antibody conjugated with FITC (sc2024, Santa Cruz Biotechnology) for 30 min at 4°C in the dark. After washing 3 times with PBST, the percentage of FITC-positive cells and mean fluorescent intensity (MFI) of FITC signals were analyzed using a FACSCanto flow cytometer (BD Biosciences) and FlowJo software (Tree Star).

Purification of soluble hTIM-1 proteins

To produce soluble hTIM-1 proteins, Expi 293F cells (Gibco) were transfected with the plasmids encoding 6 × histidine-tagged WT or 11 SNV mutants of soluble hTIM-1. The cells were cultured for 4 days and the supernatants were collected and filtered with a 0.45-μm pore membrane (Sartorius Stedim). Using the Ni-NTA purification system (Invitrogen), soluble hTIM-1 proteins were purified from the supernatants and concentrated with Amicon Ultra 50K (Merck Millipore Corporation). The purified proteins were analyzed in SDS-PAGE for their purity and then stored at −30°C until use.

Viral entry inhibition assay using soluble hTIM-1 proteins

Vero E6 cells were seeded in 96-well plates (3.0×10^4 cells per well). After overnight incubation, equal volumes of VSIVΔG*-EBOV (2,000-3,000 IUs/well) diluted in DMEM with 2% FCS and 20 μg/ml (final concentration) of purified soluble hTIM-1 proteins were mixed and incubated for 30 min at room temperature, and then added to Vero E6 cells in 5% CO_2 at 37°C. IgG S139/1 (a monoclonal antibody specific to influenza A virus hemagglutinin) was used as a negative control [86]. Twenty-four hours later, IUs were determined by counting the numbers of GFP-expressing cells with an IN Cell Analyzer 2500HS (GE Healthcare). The relative percentage of infectivity was determined by setting the IU value of cells infected with the virus alone to 100%.

Statistical analysis

All statistical analyses were performed using R software (Version 3.6.0). For the comparison of relative infectivities and expression levels of hTIM-1, one-way analysis of

variance followed by the Dunnett test was used. *p*-values of less than 0.05 were considered statistically significant.

Results

SNVs of the hTIM-1 IgV domain

I focused on the 3 loops (BC, CC', and FG) and connecting β-strands in the hTIM-1 IgV domain, which have been shown to be important for binding to EBOV GP and PS [80]. The BC, CC', and FG loops (positions 35-44, 50-59, and 101-125, respectively) are adjacent to 5 β-strands (B, C, C', F, and G at positions 31-34, 45-49, 60-64, 101-107, and 116-125, respectively) (Figs. 6b and 6c). First, amino acid positions at which SNVs had been reported were extracted (Fig. 6b). In total, 51 missense SNVs in 35 positions were found in this region. When several different amino acid residues were reported at one SNV position, the residue with the highest allele frequency of SNVs were selected and 35 missense SNVs were examined in the following experiments: 4 SNVs (S31F, V32F, T33A, and L34P) in β-strand B, 4 SNVs (P35S, Y38H, T43A, and S44P) in the BC loop, 4 SNVs (M45V, C46W, W47R, and R49S) in β-strand C, 5 SNVs (G50S, S51L, S53F, C57S, and Q58R) in the CC' loop, 2 SNVs (G60D and V62I) in β-strand C', 4 SNVs (G101D, V102L, R106H, and V107I) in β-strand F, 6 SNVs (H109P, R110C, G111R, F113L, N114S, and D115G) in the FG loop, and 6 SNVs (M116L, T119I, V120I, S121P, I124T, and V125L) in β-strand G (Figs. 6b, 6c, and Table 3).

hTIM-1 SNV substitutions affecting the entry of pseudotyped VSIV into HEK293T cells

Then, the effects of hTIM-1 SNV substitutions on the infectivities of pseudotyped VSIVs were evaluated using HEK293T cells lacking the hTIM-1 expression on the surface [63]. HEK293T cells transfected with hTIM-1-expressing plasmids were infected with VSIVΔG*-EBOV, -MARV, -LLOV, -JUNV, -LASV, or -VSIV and relative infectivities were compared to those of the cells expressing WT hTIM-1 (Fig. 7). As expected, the expression of WT hTIM-1 enhanced the cellular entry of VSIVΔG*-EBOV, -LLOV, and -JUNV, whereas weaker enhancement was seen for VSIVΔG*-MARV and -VSIV. Consistent with the previous report, VSIVΔG*-LASV infection was not enhanced by the hTIM-1 expression in HEK293T cells [13]. These results indicated that the efficiency of hTIM-1-mediated viral entry varied depending on viral surface GPs even in the same pseudotyping condition (i.e., VSIV). While none of the SNV substitutions significantly affected the infectivity of VSIVΔG*-LASV, 7 SNV substitutions (L34P, C46W, W47R, C57S, H109P, N114S, and D115G) uniformly reduced the ability of hTIM-1 to promote entry of the other pseudotyped viruses and VSIVΔG*-VSIV. On the other hand, the I124T substitution affected pseudotyped viruses (VSIVΔG*-EBOV, -MARV, -LLOV, and -JUNV) but not VSIVΔG*-VSIV. Two SNV substitutions (R110C and G111R) significantly reduced the ability of hTIM-1 against VSIVΔG*-EBOV, -LLOV, -JUNV, and -VSIV, but limited effects were observed against VSIVΔG*-MARV. In contrast, the V62I substitution only affected VSIVΔG*-JUNV. Taken together, these results indicated that most of the SNV substitutions that reduced the ability of hTIM-1-mediated viral entry were common among these viruses but that there might be a slightly different manner of action depending on the virus.

To evaluate the expression levels of exogenously introduced hTIM-1 in HEK293T cells, the band intensities were compared among WT hTIM-1 and its SNV mutant proteins in SDS-PAGE and Western blot analysis (Fig. 8a). There was no statistically significant difference in hTIM-1 expression levels compared to the value of the WT hTIM-1 molecule. I next confirmed the intracellular localization and cell surface expression levels of hTIM-1 proteins in HEK293T cells using immunofluorescence assay and flow cytometry. As expected, endogenous hTIM-1 expression was not detected in HEK293T cells, and SNV substitutions that significantly reduced the hTIM-1-mediated viral entry had no significant effect on cell surface localization of hTIM-1 proteins (Fig. 8b). The cell surface expression levels were further assessed by flow cytometry (Figs. 8c and 8d). For the percentages of FITC-positive cells and the MFI, there was no significant difference compared to WT hTIM-1 (Figs. 8c and 8d).

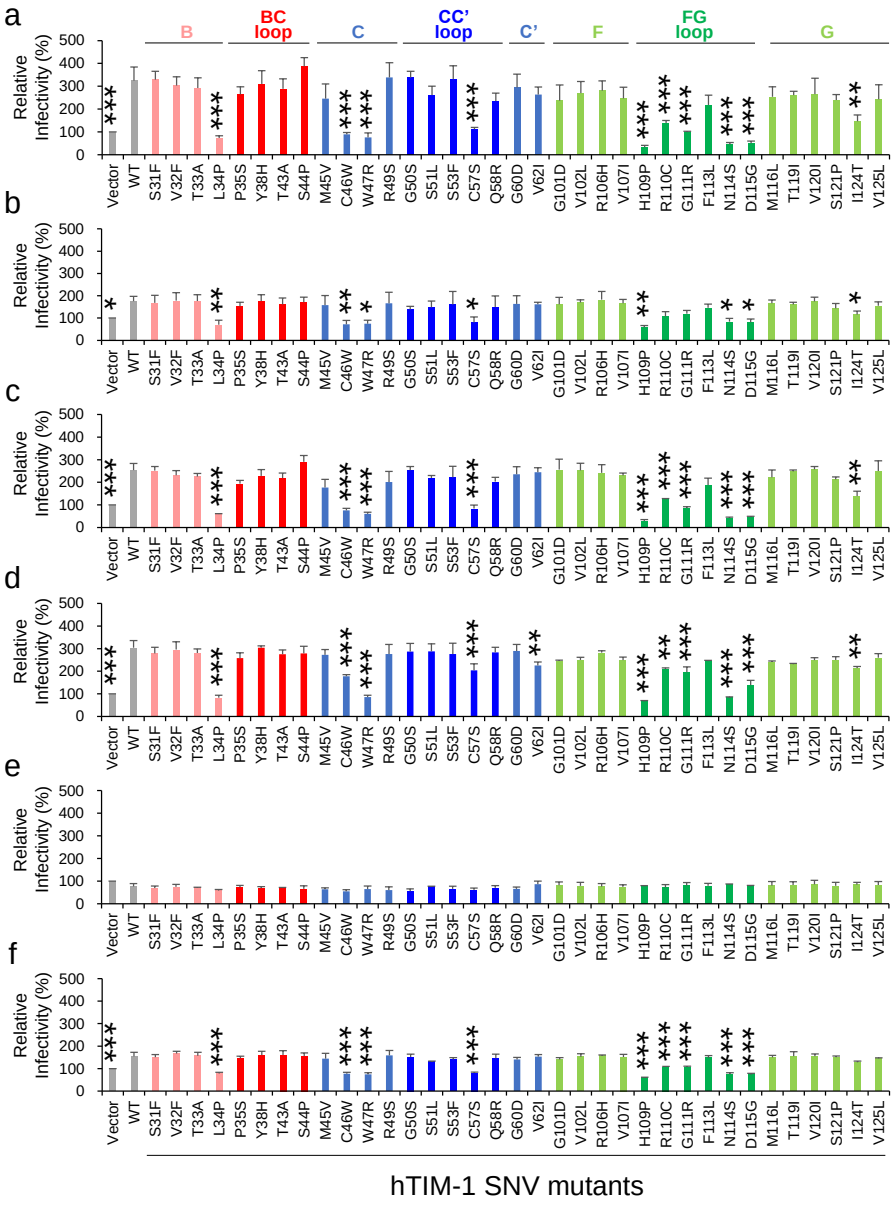

Fig. 7. Effects of 35 SNV substitutions in the hTIM-1 IgV domain on the cellular entry of pseudotyped VSIVs

HEK293T cells transfected with the plasmids encoding WT hTIM-1, its SNV mutants, or the empty plasmid were infected with VSIVΔG*-EBOV (a), -MARV (b), -LLOV (c), -JUNV (d), -LASV (e), or -VSIV (f). Twenty-four hours later, IUs were determined by counting the numbers of GFP-positive cells and the relative infectivities were determined by setting the IU value of empty plasmid-transfected cells to 100%. The means and SDs of 3 independent experiments are shown. Statistical significance was calculated compared to WT using the Dunnett test (*$p < 0.05$, **$p < 0.01$, ***$p < 0.001$).

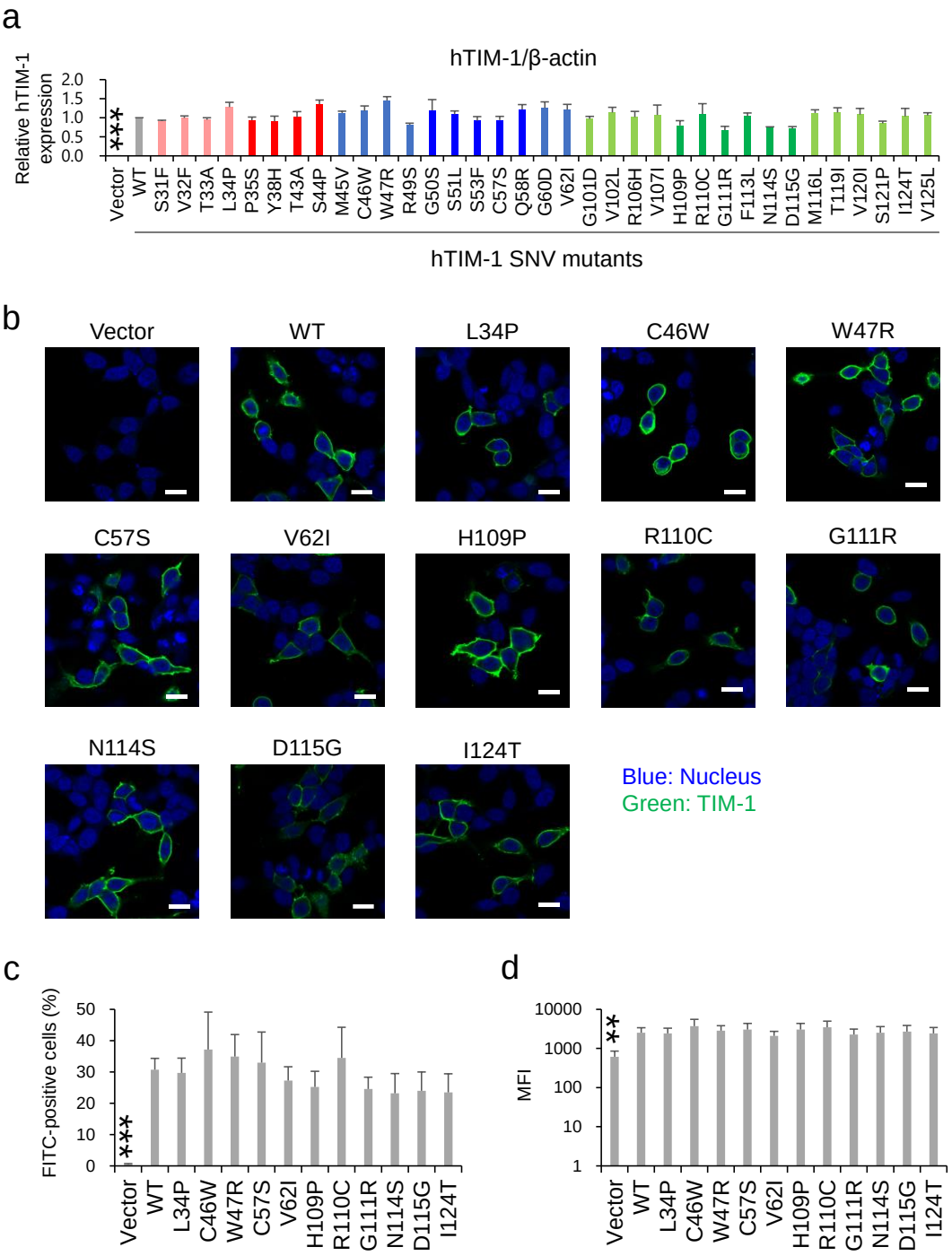

Fig. 8. Expression levels of exogenous hTIM-1 proteins in HEK293T cells

(a) HEK293T cells transfected with the plasmids encoding WT hTIM-1, its SNV mutants, or the empty plasmid were harvested at 48 hours post-transfection and analyzed in SDS-PAGE and Western blotting. The amounts of β-actin in the total cell lysates were also analyzed as an internal control. The relative expression level was determined as the ratio of the band intensity of hTIM-1 to β-actin, and that of each SNV mutant was compared

with that of WT hTIM-1. The means and SDs of 3 independent experiments are shown. Statistical significance was calculated compared to WT using the Dunnett test (***p < 0.001). (b) HEK293T cells transfected with the plasmids encoding WT hTIM-1, its SNV mutants, or empty plasmid were immunostained as described in the Materials and Methods section. The cell images were captured with confocal microscopy. The scale bars represent 10 μm. (c and d) HEK293T cells transfected with the plasmids and immunostained as described above were also analyzed with a FACSCanto flow cytometer. The cell surface expression of hTIM-1 was quantified as percentages of the FITC-positive cells (c) and MFI of the FITC signals (d). Statistical significance was calculated compared to the WT using the Dunnett test (**p < 0.01, ***p < 0.001).

SNV substitutions affecting neutralizing activity of soluble hTIM-1 against VSIVΔG*-EBOV

hTIM-1 expressed on the cell membrane is cleaved by a matrix metalloproteinase upstream of the transmembrane domain, resulting in the production of the soluble form of hTIM-1 [87,88]. Soluble forms of hTIM-1 are reported to inhibit some viral infections and are expected to be therapeutic candidates [70,72,89–91]. To further assess the effects of SNV substitutions on viral entry, purified soluble hTIM-1 proteins containing each representative SNV substitution were produced and their neutralizing activities against VSIVΔG*-EBOV were compared (Fig. 9). As expected, the soluble form of WT hTIM-1 significantly inhibited viral infection by about 50%, whereas no inhibitory effect was seen in a negative control (CTR IgG). Soluble hTIM-1 proteins with the V62I substitution also significantly inhibited infection as efficiently as WT hTIM-1, suggesting that this substitution did not significantly affect the hTIM-1 function consistent with the data of cellular entry assay for VSIVΔG*-EBOV (Fig. 7). On the other hand, the other 10 SNVs tested for soluble forms, all of which significantly reduced the infectivity of VSIVΔG*-EBOV as described above (see Fig. 7), showed less ability to inhibit VSIVΔG*-EBOV infection than WT and V62I hTIM-1. Indeed, no significant differences compared to CTR IgG were detected in 8 of the 10 SNV mutants, and only slight inhibitory activity was detected in 2 SNV substitutions (N114S and I124T).

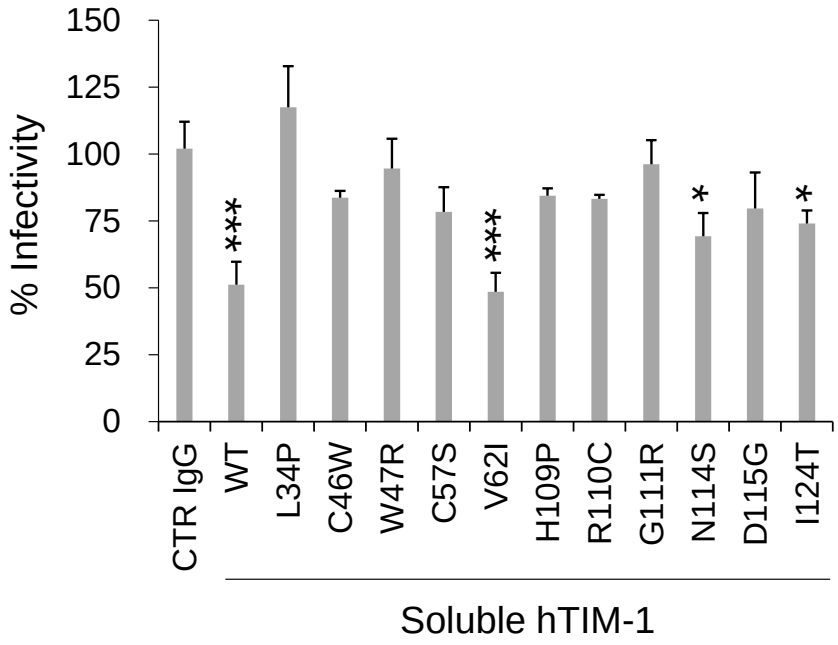

Fig. 9. Effects of SNV substitutions on the ability of soluble hTIM-1 to inhibit cellular entry of VSIVΔG*-EBOV into Vero E6 cells

Vero E6 cells were infected with VSIVΔG*-EBOV preincubated with 20 μg/ml soluble forms of WT hTIM-1 or its SNVs mutants for 30 min at room temperature. An anti-influenza A virus hemagglutinin monoclonal antibody was used as a negative control (CTR IgG). After 24-hour incubation, GFP-positive cells were counted. The relative percentage of infectivity was calculated by setting the IU value of cells infected with virus alone to 100%. Each bar represents the means and SDs of triplicate wells. Statistical significance was calculated compared to CTR IgG using the Dunnett test (*$p < 0.05$, ***$p < 0.001$).

Mapping of the hTIM-1 SNV positions

In total, 11 SNV substitutions in the hTIM-1 IgV domain (L34P, C46W, W47R, C57S, V62I, H109P, R110C, G111R, N114S, D115G, and I124T) were found to reduce the hTIM-1-mediated cellular entry of the pseudotyped VSIVs (Fig. 7). Structural analyses revealed that the amino acid residues at positions 57, 109, 110, 111, 114, 115, and 124 were exposed on the surface of the IgV domain, whereas the amino acid residues at positions 34, 46, 47, and 62 were not located on the molecular surface (Fig. 10). Of these, 5 SNV positions (109, 110, 111, 114, and 115) were located around the PS-binding site (MILBS motif, 112-115) in the FG loop. On the other hand, 6 SNV positions (34, 46, 47, 57, 62, and 124) were located far from this site. Position 34 was located on the boundary between β-strand B and the BC loop, positions 46 and 47 were located on β-strand B, and position 57 was located on the CC' loop. Two cysteine residues at positions 46 and 57 forming a disulfide bond bridged the CC' loop and the GFC β-sheet [78]. Positions 62 and 124 were located on β-strands C' and G, respectively.

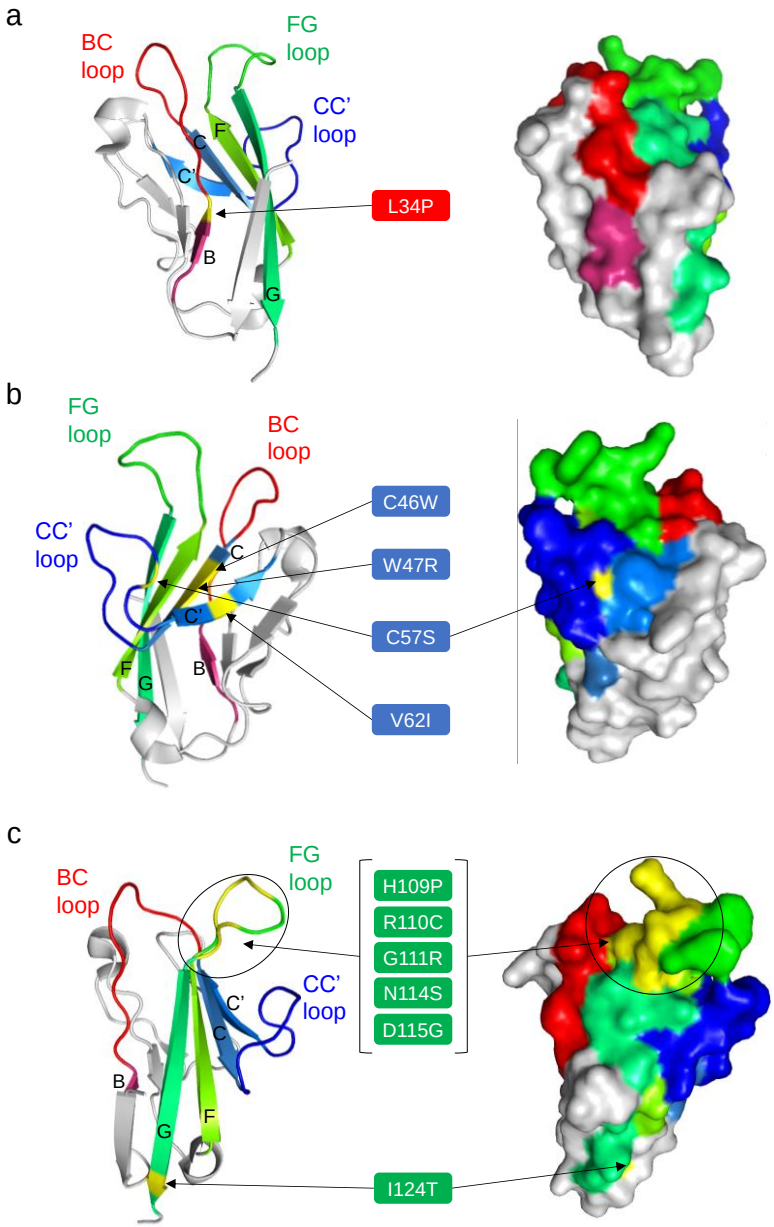

Fig. 10. Amino acid positions of the hTIM-1 SNV substitutions that significantly reduced the ability to promote the cellular entry of the pseudotyped viruses

The amino acid positions of the 11 SNV substitutions that reduced the cellular entry of VSIV-based pseudotyped viruses in the present study are shown in yellow in the crystal structure of the IgV domain in the hTIM-1 molecule (PDB ID: 5DZO). Other coloring is the same as in Fig. 1. To focus on these amino acid positions and locations of the BC, CC', and FG loops, the 11 SNVs were separately mapped in 3 figures; BC loop (a), CC' loop (b), and FG loop (c). Ribbon (left panel) and surface (right panel) representations of the hTIM-1 IgV domain are shown. In the left panels, 5 β-strands (B, C, C', F, and G) are indicated with their corresponding letters.

Allele frequencies and functional predictions of hTIM-1 SNVs

It is found that the allele frequencies of most of the SNVs examined in this study were very low in the global population (Table 4 and 5). The W47R variant with the highest MAF among the SNVs was also found to be a rare variant (MAF = 1.44×10^{-4}). Then, potential modifications of the hTIM-1 structure caused by the SNV substitutions were predicted using bioinformatics tools, including SIFT, PolyPhen-2, CADD, and REVEL from the Ensembl genome browser (Table 4). The V62I substitution was predicted to have no effect on the protein structure, whereas L34P, C46W, W47R, C57S, and D115G SNV substitutions were predicted to disrupt the functional structure by all the bioinformatics tools used in this study. G111R, N114S, and I124T substitutions were predicted to have some negative effects by SIFT, PolyPhen-2, and CADD, whereas H109P and R110C substitutions were predicted to damage the hTIM-1 structure only by SIFT and PolyPhen-2. In summary, among the 11 SNV substitutions that reduced the TIM-1-mediated viral entry, 10 substitutions were predicted to likely have the potential to alter the hTIM-1 function. In contrast, SNV substitutions that had no significant effect on viral entry showed a tendency to be predicted to cause a mild or no change in its function (Table 5).

Table 4. Information of hTIM-1 SNV substitutions that significantly reduced the cellular entry of pseudotyped viruses

SNVs	Global MAF[a]	SIFT[b]	PolyPhen-2[c]	CADD[d]	REVEL[e]
L34P	7.39×10^{-5}	D	ProD	LD	LDC
C46W	3.94×10^{-5}	D	ProD	LD	LDC
W47R	1.44×10^{-4}	D	ProD	LD	LDC
C57S	6.57×10^{-6}	D	ProD	LD	LDC
V62I	3.94×10^{-5}	T	B	LB	LB
H109P	4.02×10^{-6}	D	PosD	LB	LB
R110C	1.97×10^{-5}	D	PosD	LB	LB
G111R	6.57×10^{-6}	D	ProD	LD	LB
N114S	4.09×10^{-6}	D	ProD	LD	LB
D115G	2.63×10^{-5}	D	ProD	LD	LDC
I124T	7.96×10^{-6}	D	ProD	LD	LB

[a]MAFs of hTIM-1 SNVs were obtained from gnomAD and TOPMed. [b]SIFT: Sorting intolerant from tolerant, D: Deleterious, T: Tolerated [c]PolyPhen-2: Polymorphism phenotyping-2, B: Benign, PosD: Possibly damaging, ProD: Probably damaging [d]CADD: Combined annotation dependent depletion, LB: Likely benign, LD: Likely deleterious [e]REVEL: Rare exome variant ensemble learner, LB: Likely benign, LDC: Likely disease-causing

Table 5. Information of hTIM-1 SNV substitutions that did not significantly affect the cellular entry of pseudotyped viruses

SNVs	Global MAF[a]	SIFT[b]	PolyPhen-2[c]	CADD[d]	REVEL[e]
S31F	NA[f]	D	PosD	LB	LB
V32F	NA	D	ProD	LB	LB
T33A	6.57×10^{-6}	D	PosD	LB	LB
P35S	6.57×10^{-6}	T	PosD	LB	LB
Y38H	NA	D	ProD	LD	LB
T43A	4.01×10^{-6}	D	B	LB	LB
S44P	4.01×10^{-6}	D	B	LB	LB
M45V	1.00×10^{-4}	D	PosD	LB	LB
R49S	6.57×10^{-6}	D	ProD	LB	LB
G50S	4.01×10^{-6}	D	ProD	LB	LB
S51L	3.28×10^{-5}	D	B	LD	LB
S53F	4.00×10^{-6}	D	PosD	LD	LB
Q58R	4.01×10^{-6}	T	B	LB	LB
G60D	2.00×10^{-5}	T	B	LB	LB
G101D	4.00×10^{-6}	D	PosD	LD	LDC
V102L	3.29×10^{-5}	T	B	LB	LB
R106H	3.29×10^{-5}	D	ProD	LD	LDC
V107I	NA	T	B	LB	LB
F113L	2.63×10^{-5}	D	ProD	LD	LB
M116L	1.25×10^{-5}	T	B	LB	LB
T119I	4.20×10^{-6}	D	PosD	LB	LB
V120I	4.60×10^{-5}	T	B	LB	LB
S121P	6.57×10^{-6}	D	ProD	LB	LB
V125L	1.97×10^{-5}	D	B	LB	LB

[a-e]The abbreviations and criteria are described in the footnote of Table 4. [f]NA: Information is not available in the databases.

Discussion

It has been reported that polymorphisms of hTIM-1 are associated with the pathogenesis of atopic dermatitis, allergy, rheumatoid arthritis, asthma, systemic lupus erythematosus, and viral infections [92–94]. Since hTIM-1 is one of the major attachment receptors for some viruses, substitutions in hTIM-1 SNVs might influence the susceptibility of humans to viral infections. However, the information on hTIM-1 SNVs affecting virus infectivity is still limited. Here, I focused on 35 missense SNV substitutions located in the hTIM-1 IgV domain and found that some SNVs might have reduced ability to promote virus infections.

The PS-binding activity of the IgV domain is thought to be important for the attachment of some enveloped viruses, and the PS-binding site was identified as MILIBS consisting of 4 amino acid residues (WFND motif: W112, F113, N114, and D115) in the FG loop [78,79]. Accordingly, N114D and D115A substitutions in this motif were shown to abolish flavivirus infection [95]. Consistent with this previous finding, 5 SNV substitutions, N114S, and D115G, as well as H109P, R110C, and G111R, N114S, around the PS-binding site in the FG loop influenced the cellular entry of the pseudotyped VSIV (Figs. 7 and 10c). These SNV substitutions may directly alter the PS-binding site, resulting in the reduced ability of hTIM-1 to interact with PS on the viral envelope.

Five SNV substitutions (L34P, C46W, W47R, C57S, and V62I) between β-strands B and C', which are not directly involved in the PS-binding pocket, also reduced the viral entry into cells. In addition, 4 of these amino acids (i.e., positions 34, 46, 47, and 62) are not even exposed on the surface of the hTIM-1 molecule. It is assumed that these SNV substitutions might potentially cause structural distortions of the IgV domain, leading to reduced interaction with PS and/or viral GPs. For example, the L34P substitution might affect the flexibility of the BC loop since this amino acid position is located at the root of the BC loop inside the molecule (Fig. 10a). The C46W and C57S substitutions might also alter the conformation of the molecule since these amino acid substitutions abolish the disulfide bond (C46-C57) between β-strand C and the FG loop, which plays an important role in maintaining the PS-binding pocket [78]. It is previously reported that single amino acid substitutions at position 48 in African green monkey-derived TIM-1 affected the infectivity of VSIVs pseudotyped with filovirus GPs [76]. Interestingly, this position is close to the 2 SNV substitutions (C46W and W47R in β-strand C), resulting in the reduction of the virus infectivity in the present study, suggesting that these consecutive amino acid residues (i.e., positions 46-48) are important for the hTIM-1 function as an attachment receptor for viral infection.

Interestingly, the I124T substitution in β-strand G connecting to the FG loop reduced

the viral entry. Although this amino acid position is located far from the PS-binding site, the I124T substitution might affect the stability of the FG loop, indirectly reducing the PS-binding activity. It might also be possible that the I124T substitution reduced the interaction with EBOV, MARV, LLOV, and JUNV GPs since the infectivity of VSIVΔG*-VSIV was only limitedly affected by this substitution. It was also noted that the V62I substitution significantly reduced the cellular entry of VSIVΔG*-JUNV but not the other viruses. It is also noted that the S51L substitution reduced the hTIM-1-mediated enhancement of pseudotyped lentivirus bearing chikungunya virus GP [75], but this substitution resulted in no significant change in the VSIV pseudotyped with filovirus and arenavirus GP in the present study. A previous study demonstrated that hTIM-1 binds to the receptor binding domain of EBOV GP in addition to PS, although the interaction site between EBOV GP and hTIM-1 is still elusive [80]. Importantly, the present data may also suggest the mechanisms underlying the binding of hTIM-1 to viral GPs. Crystal structures of the complex of GPs and hTIM-1 will be needed to determine its molecular basis.

It was found that the expression of WT hTIM-1 significantly enhanced the cellular entry of VSIVΔG*-JUNV but not -LASV in HEK293T cells (Fig. 7). This difference might be attributed to the differences in the host cell receptors for these arenaviruses. JUNV and LASV are known to utilize transferrin receptor 1 and α-dystroglycan (αDG) as attachment receptors on the cell surface, respectively [13,96]. A previous study demonstrated that the exogenous hTIM-1 expression enhanced the entry of VSIVΔG*-LASV in αDG-knockout HEK293T cells but not in original HEK293T cells [96]. From these findings, they suggested that VSIVΔG*-LASV might bind to αDG more efficiently than hTIM-1, and hTIM-1 might serve as an attachment factor for LASV only in the absence of functional αDG. In the present study, although none of the hTIM-1 molecules significantly enhanced the VSIVΔG*-LASV infectivity in HEK293T cells, the entry of this virus might be affected if using different cell lines such as an αDG-knockout cells. Additional studies are needed to clarify the significance of hTIM-1 SNVs on arenavirus infections.

In another study that investigated single amino acid substitutions in the hTIM-1 IgV domain using an alanine scanning method, 8 substitutions (Y38A, F55A, R106A, G111A, F113A, N114A, D115A, and K117A located on the BC, CC' and FG loops) were found to decrease the efficiency of GP-mediated EBOV entry into cells [71]. However, no significant change in the VSIVΔG*-EBOV infectivity was found in the hTIM-1 SNV mutants with Y38H and R106H substitutions in the present study, while 2 substitutions (H109A and R110A located on the FG loop) that affected the virus infectivity in the

present study did not decrease the GP-mediated EBOV entry into cells in a previous study [71]. Such differences suggested that the polarity of amino acids at these positions may be important for the interaction between hTIM-1 and PS and/or viral GPs.

The present study suggests that hTIM-1 polymorphisms may affect cell susceptibility to viral infections. Eleven SNV substitutions were found to reduce the cellular entry of VSIV pseudotyped viruses, but it is indeed still unclear which process (i.e., viral attachment, internalization, or membrane fusion) was affected by these substitutions. Although these SNV substitutions are thought to reduce viral attachment, further studies are needed to clarify the mechanisms of the SNV-associated dysfunction of hTIM-1. Another limitation of this study is that pseudotyped VSIVs were used, and the hTIM-1-mediated cellular entry might be largely dependent on the VSIV envelope. I assume that biological properties, such as the lipid composition of the envelope and density of viral glycoproteins on the viral particle, are different between pseudotyped VSIVs and authentic filoviruses/arenaviruses. To further investigate the association of genetic polymorphisms in hTIM-1 and viral infections, both *in vitro* and *in vivo* experiments using the authentic viruses are needed in the future. It would also be of interest to investigate the hTIM-1 SNVs for other physiological roles such as immune-regulatory function.

Summary

hTIM-1 is known to promote cellular entry of enveloped viruses. Previous studies suggested that the polymorphisms of hTIM-1 affected its function. Here, SNVs of hTIM-1 were analyzed to determine their ability to promote cellular entry of viruses, using pseudotyped VSIV. hTIM-1 sequences were obtained from a public database (Ensembl genome browser) and 35 missense SNVs in 3 loops of the hTIM-1 IgV domain were identified, which had been reported to interact with the Ebola virus glycoprotein GP and PS in the viral envelope. HEK293T cells transiently expressing wildtype hTIM-1 or its SNV mutants were infected with VSIVs pseudotyped with filovirus or arenavirus GPs, and their infectivities were compared. Eleven of the thirty-five SNV substitutions reduced the efficiency of hTIM-1-mediated entry of pseudotyped VSIVs. These SNV substitutions were found not only around the PS-binding pocket but also in other regions of the molecule. Taken together, these results suggest that some SNVs of the hTIM-1 IgV domain have impaired ability to interact with PS and/or viral GPs in the viral envelope, which may affect the hTIM-1 function to promote viral entry into cells.

Conclusion

It has been suggested that the genetic polymorphisms of host cell receptors might be one of the factors affecting the susceptibility of humans to viral infections. However, the genetic polymorphisms such as SNVs that potentially influence cell susceptibilities to SARS-CoV-2 and hemorrhagic fever viruses have not been fully characterized. In this thesis, I focused on the effects of the SNV substitutions of host cell receptors on cell susceptibilities to these viruses.

In Chapter I, I investigated SNVs of human ACE2, the principal receptor of SARS-CoV and SARS-CoV-2, and demonstrated that some ACE2 SNV substitutions affected the cell susceptibility to these CoVs. Since previous studies suggested that 29 SNV substitutions in ACE2 altered the binding affinity between ACE2 and RBD of the SARS-CoV-2 S protein, I analyzed the actual effects of these SNV substitutions on the cellular entry of SARS-CoV and SARS-CoV-2 using pseudotyped VSIVs and found that some of the SNV substitutions positively or negatively affected the entry of these CoVs into cells. By further assessing the infectivities of SARS-CoV-2 VOCs in the same way, it was found that the effects of the ACE2 SNV substitutions might be slightly different among VOCs. The ACE2 SNV substitutions that affected the entry of these viruses were found at the amino acid positions reported to be important for the interactions with the viral S protein and also at some other positions that were involved in the stabilization of the ACE2 structure. The present data support the notion that human ACE2 SNVs that influence the affinity to the S protein and/or the overall structure of the ACE2 molecule may affect cell susceptibilities to SARS-CoV and SARS-CoV-2 including VOCs.

In Chapter II, SNVs in the hTIM1 molecule, which is known as an attachment receptor for enveloped viruses, were investigated. I focused on 35 SNVs in 3 loops of the hTIM1 IgV domain, which interact with EBOV GP and PS in the viral envelope and demonstrated that 11 of the 35 SNV substitutions reduced the ability to promote the cellular entry of VSIVs pseudotyped with filovirus and arenavirus GPs. Furthermore, soluble forms of hTIM-1 proteins containing each SNV substitution that significantly reduced the entry of VSIV pseudotyped with EBOV showed less neutralizing activities against this virus. Of the amino acid positions associated with the 11 SNVs, 5 positions were found to be located on the PS binding site and 6 positions located far from this site. Taken together, these results suggest that the 11 SNVs of the hTIM-1 molecule have impaired function to interact with PS and/or viral GPs and may influence cell susceptibilities to filovirus and arenavirus infections.

The present thesis provides the evidence that SNVs of host cell receptors are potentially one of the molecular factors affecting cell susceptibilities to viral infections.

This study includes information on not only the SNVs related to reduced or enhanced viral entry into cells but also the mechanisms underlying the binding of viral proteins to host cell receptors and will be of interest to a cross-section of the researchers in virology, molecular biology, and genetics. Further studies such as large-scale epidemiological surveys of genetic variations on this topic will be needed to confirm the significance of genetic polymorphisms on the pathogenesis of viral infections.

Acknowledgements

I would like to express my sincere gratitude to my boss, Prof. Ayato Takada (Division of Global Epidemiology, International Institute for Zoonosis Control [IIZC], Hokkaido University [HU], Sapporo, Japan). He gave me continuous support for my experiments, many accurate advice and guidance during my Ph.D. course and a lot of opportunities for my growth.

I sincerely appreciate helpful advice and suggestions from Prof. Hirofumi Sawa (Division of Molecular Pathobiology, IIZC, HU), Prof. Hiroaki Kariwa (Laboratory of Public Health, School/Faculty of Veterinary Medicine, HU), and Prof. Yoshihiro Sakoda (Laboratory of Microbiology, School/Faculty of Veterinary Medicine, HU).

I would like to thank the coordinator at the World-leading Innovative and Smart Education (WISE) Program, Prof. Motohiro Horiuchi (Laboratory of Veterinary Hygiene, School/Faculty of Veterinary Medicine, HU), and the members of the WISE Program Office for their help with my Ph.D. coursework.

I would like to specially thank to Associate Prof. Manabu Igarashi, Assistant Prof. Masahiro Kajihara (Division of Global Epidemiology, IIZC, HU), Assistant Prof. Rashid Manzoor (Higher Colleges of Technology, Abu Dhabi, United Arab Emirates), and Dr. Michihito Sasaki (Division of Molecular Pathobiology, IIZC, HU) for their assistance, intellectual advice, and warm support.

The following people helpfully provided technical and academic advice and kind daily support: Ms. Hiroko Miyamoto, Ms. Akina Mori-Kajihara, Ms. Kanako Ibaraki, Mr. Suguru Taga, Dr. Yoshiro Takadate, Dr. Takeshi Saito, Dr. Kosuke Okuya, Dr. Mao Isono, Dr. Boniface Lombe Pongombo, Ms. Yurie Kida, Ms. Nodoka Kasajima, Mr. Yuji Takahashi, Dr. Yannick Munyeku Bazitama, Ms. Risa Hayashi, and Dr. Francois Edidi Atani (Division of Global Epidemiology, IIZC, HU).

I am deeply grateful to thank the staff members of Asahikawa pain clinic hospital, especially Dr. Mitsuaki Matoba and Dr. Kotaro Matoba.

Finally, I can never express my gratitude enough for all my family members and the staff members of Hattori Clinic, have done for me. I owe my life to them.

References

1. You, Y.; Yang, X.; Hung, D.; Yang, Q.; Wu, T.; Deng, M. Asymptomatic COVID-19 infection: Diagnosis, transmission, population characteristics. *BMJ Support. Palliat. Care* **2021**, *0*, 1–8.
2. Dean, N.E.; Halloran, M.E.; Yang, Y.; Longini, I.M. Transmissibility and pathogenicity of Ebola virus: A systematic review and meta-analysis of household secondary attack rate and asymptomatic infection. *Clin. Infect. Dis.* **2016**, *62*, 1277–1286.
3. Paessler, S.; Walker, D.H. Pathogenesis of the viral hemorrhagic fevers. *Annu. Rev. Pathol. Mech. Dis.* **2013**, *8*, 411–440.
4. Yun, N.E.; Walker, D.H. Pathogenesis of Lassa fever. *Viruses* **2012**, *4*, 2031–2048.
5. Shastry, B.S. SNPs in disease gene mapping, medicinal drug development and evolution. *J. Hum. Genet.* 2007, *52*, 871–880.
6. Shastry, B.S.; Shastry, B.S. SNP alleles in human disease and evolution. *J Hum Genet* **2002**, *47*, 561–566.
7. Katsonis, P.; Koire, A.; Wilson, S.J.; Hsu, T.-K.; Lua, R.C.; Wilkins, A.D.; Lichtarge, O. Single nucleotide variations: Biological impact and theoretical interpretation. *Protein Sci.* **2014**, *23*, 1650–1666.
8. Weerd, N.A.; Vivian, J.P.; Lim, S.S.; Huang, S.U.; Hertzog, P.J. Structural integrity with functional plasticity: What type I IFN receptor polymorphisms reveal. *J. Leukoc. Biol.* **2020**, *108*, 909–924.
9. Schröder, N.W.; Schumann, R.R. Single nucleotide polymorphisms of Toll-like receptors and susceptibility to infectious disease. *Lancet Infect. Dis.* **2005**, *5*, 156–164.
10. Nogales, A.; L. DeDiego, M. Host single nucleotide polymorphisms modulating influenza A virus disease in humans. *Pathogens* **2019**, *8*, 168.
11. Evans, J.P.; Liu, S. Role of host factors in SARS-CoV-2 entry. *J. Biol. Chem.* **2021**, *297*, 100847.
12. White, J.M.; Schornberg, K.L. A new player in the puzzle of filovirus entry. *Nat. Rev. Microbiol.* **2012**, *10*, 317–322.
13. Jemielity, S.; Wang, J.J.; Chan, Y.K.; Ahmed, A.A.; Li, W.; Monahan, S.; Bu, X.; Farzan, M.; Freeman, G.J.; Umetsu, D.T.; et al. TIM-family proteins promote infection of multiple enveloped viruses through virion-associated phosphatidylserine. *PLoS Pathog.* **2013**, *9*, e1003232.
14. Wang, C.; Li, W.; Drabek, D.; Okba, N.M.A.; van Haperen, R.; Osterhaus,

A.D.M.E.; van Kuppeveld, F.J.M.; Haagmans, B.L.; Grosveld, F.; Bosch, B.-J. A human monoclonal antibody blocking SARS-CoV-2 infection. *Nat. Commun.* **2020**, *11*, 2251.

15. Li, W.; Wong, S.-K.; Li, F.; Kuhn, J.H.; Huang, I.-C.; Choe, H.; Farzan, M. Animal origins of the severe acute respiratory syndrome coronavirus: Insight from ACE2-S-protein interactions. *J. Virol.* **2006**, *80*, 4211–4219.
16. Yi, C.; Sun, X.; Ye, J.; Ding, L.; Liu, M.; Yang, Z.; Lu, X.; Zhang, Y.; Ma, L.; Gu, W.; et al. Key residues of the receptor binding motif in the spike protein of SARS-CoV-2 that interact with ACE2 and neutralizing antibodies. *Cell. Mol. Immunol.* **2020**, *17*, 621–630.
17. Hoffmann, M.; Kleine-Weber, H.; Schroeder, S.; Krüger, N.; Herrler, T.; Erichsen, S.; Schiergens, T.S.; Herrler, G.; Wu, N.H.; Nitsche, A.; et al. SARS-CoV-2 cell entry depends on ACE2 and TMPRSS2 and is blocked by a clinically proven protease inhibitor. *Cell* **2020**, *181*, 271-280.e8.
18. Shukla, N.; Roelle, S.M.; Suzart, V.G.; Bruchez, A.M.; Matreyek, K.A. Mutants of human ACE2 differentially promote SARS-CoV and SARS-CoV-2 spike mediated infection. *PLOS Pathog.* **2021**, *17*, e1009715.
19. Joshi, N.; Tyagi, A.; Nigam, S. Molecular level dissection of critical spike mutations in SARS-CoV-2 variants of concern (VOCs): A simplified review. *ChemistrySelect* **2021**, *6*, 7981–7998.
20. Huang, S.W.; Wang, S.F. SARS-CoV-2 entry related viral and host genetic variations: Implications on covid-19 severity, immune escape, and infectivity. *Int. J. Mol. Sci.* **2021**, *22*, 1–22.
21. Gupta, R.; Misra, A. COVID19 in South Asians/Asian Indians: Heterogeneity of data and implications for pathophysiology and research. *Diabetes Res. Clin. Pract.* **2020**, *165*, 108267.
22. Hashemi, S.M.A.; Thijssen, M.; Hosseini, S.Y.; Tabarraei, A.; Pourkarim, M.R.; Sarvari, J. Human gene polymorphisms and their possible impact on the clinical outcome of SARS-CoV-2 infection. *Arch. Virol.* **2021**, *166*, 2089–2108.
23. Hamming, I.; Timens, W.; Bulthuis, M.; Lely, A.; Navis, G.; van Goor, H. Tissue distribution of ACE2 protein, the functional receptor for SARS coronavirus. A first step in understanding SARS pathogenesis. *J. Pathol.* **2004**, *203*, 631–637.
24. Wiese, O.; Zemlin, A.E.; Pillay, T.S. Molecules in pathogenesis: Angiotensin converting enzyme 2 (ACE2). *J. Clin. Pathol.* **2021**, *74*, 285–290.
25. Chen, J.; Jiang, Q.; Xia, X.; Liu, K.; Yu, Z.; Tao, W.; Gong, W.; Han, J.J. Individual variation of the SARS-CoV-2 receptor ACE2 gene expression and

regulation. *Aging Cell* **2020**, *19*, 1–12.
26. Singh, H.; Choudhari, R.; Nema, V.; Khan, A.A. ACE2 and TMPRSS2 polymorphisms in various diseases with special reference to its impact on COVID-19 disease. *Microb. Pathog.* **2021**, *150*, 104621.
27. Calcagnile, M.; Forgez, P.; Iannelli, A.; Bucci, C.; Alifano, M.; Alifano, P. Molecular docking simulation reveals ACE2 polymorphisms that may increase the affinity of ACE2 with the SARS-CoV-2 spike protein. *Biochimie* **2021**, *180*, 143–148.
28. Hashizume, M.; Gonzalez, G.; Ono, C.; Takashima, A.; Iwasaki, M. Population-specific ACE2 single-nucleotide polymorphisms have limited impact on SARS-CoV-2 infectivity in vitro. *Viruses* **2021**, *13*, 1–10.
29. Chan, K.K.; Dorosky, D.; Sharma, P.; Abbasi, S.A.; Dye, J.M.; Kranz, D.M.; Herbert, A.S.; Procko, E. Engineering human ACE2 to optimize binding to the spike protein of SARS coronavirus 2. *Science.* **2020**, *369*, 1261–1265.
30. Darbani, B. The expression and polymorphism of entry machinery for covid-19 in human: Juxtaposing population groups, gender, and different tissues. *Int. J. Environ. Res. Public Health* **2020**, *17*, 3433.
31. National Centre for Biotechnological Information SNP Available online: https://www.ncbi.nlm.nih.gov/snp/ (accessed on Dec 1, 2021).
32. Takada, A.; Robison, C.; Goto, H.; Sanchez, A.; Murti, K.G.; Whitt, M.A.; Kawaoka, Y. A system for functional analysis of Ebola virus glycoprotein. *Proc. Natl. Acad. Sci.* **1997**, *94*, 14764–14769.
33. Nie, J.; Li, Q.; Wu, J.; Zhao, C.; Hao, H.; Liu, H.; Zhang, L.; Nie, L.; Qin, H.; Wang, M.; et al. Establishment and validation of a pseudovirus neutralization assay for SARS-CoV-2. *Emerg. Microbes Infect.* **2020**, *9*, 680–686.
34. Zhang, F.; Li, W.; Feng, J.; Ramos da Silva, S.; Ju, E.; Zhang, H.; Chang, Y.; Moore, P.S.; Guo, H.; Gao, S. SARS-CoV-2 pseudovirus infectivity and expression of viral entry-related factors ACE2, TMPRSS2, Kim-1, and NRP-1 in human cells from the respiratory, urinary, digestive, reproductive, and immune systems. *J. Med. Virol.* **2021**, *93*, 6671–6685.
35. Schrom, E.; Huber, M.; Aneja, M.; Dohmen, C.; Emrich, D.; Geiger, J.; Hasenpusch, G.; Herrmann-Janson, A.; Kretzschmann, V.; Mykhailyk, O.; et al. Translation of angiotensin-converting enzyme 2 upon liver- and lung-targeted delivery of optimized chemically modified mRNA. *Mol. Ther. Nucleic Acids* **2017**, *7*, 350–365.
36. Ng, K.W.; Attig, J.; Bolland, W.; Young, G.R.; Major, J.; Wrobel, A.G.;

Gamblin, S.; Wack, A.; Kassiotis, G. Tissue-specific and interferon-inducible expression of nonfunctional ACE2 through endogenous retroelement co-option. *Nat. Genet.* **2020**, *52*, 1294–1302.

37. Nakayama, E.; Tomabechi, D.; Matsuno, K.; Kishida, N.; Yoshida, R.; Feldmann, H.; Takada, A. Antibody-dependent enhancement of Marburg virus infection. *J. Infect. Dis.* **2011**, *204*, S978–S985.
38. Puray-Chavez, M.; LaPak, K.M.; Schrank, T.P.; Elliott, J.L.; Bhatt, D.P.; Agajanian, M.J.; Jasuja, R.; Lawson, D.Q.; Davis, K.; Rothlauf, P.W.; et al. Systematic analysis of SARS-CoV-2 infection of an ACE2-negative human airway cell. *Cell Rep.* **2021**, *36*, 109364.
39. Niu, W.; Qi, Y.; Hou, S.; Zhou, W.; Qiu, C. Correlation of angiotensin-converting enzyme 2 gene polymorphisms with stage 2 hypertension in Han Chinese. *Transl. Res.* **2007**, *150*, 374–380.
40. Pal, R.; Bhansali, A. COVID-19, diabetes mellitus and ACE2: The conundrum. *Diabetes Res. Clin. Pract.* **2020**, *162*, 108132.
41. Crackower, M.A.; Sarao, R.; Oliveira-dos-Santos, A.J.; Da Costa, J.; Zhang, L. Angiotensin-converting enzyme 2 is an essential regulator of heart function. *Nature* **2002**, *417*, 822–828.
42. Saih, A.; Baba, H.; Bouqdayr, M.; Ghazal, H.; Hamdi, S.; Kettani, A.; Wakrim, L. In silico analysis of high-risk missense variants in human ACE2 gene and susceptibility to SARS-CoV-2 infection. *Biomed Res. Int.* **2021**, *2021*, 1–10.
43. Hussain, M.; Jabeen, N.; Raza, F.; Shabbir, S.; Baig, A.A.; Amanullah, A.; Aziz, B. Structural variations in human ACE2 may influence its binding with SARS-CoV-2 spike protein. *J. Med. Virol.* **2020**, *92*, 1580–1586.
44. Suryamohan, K.; Diwanji, D.; Stawiski, E.W.; Gupta, R.; Miersch, S.; Liu, J.; Chen, C.; Jiang, Y.P.; Fellouse, F.A.; Sathirapongsasuti, J.F.; et al. Human ACE2 receptor polymorphisms and altered susceptibility to SARS-CoV-2. *Commun. Biol.* **2021**, *4*, 475.
45. Paniri, A.; Hosseini, M.M.; Moballegh-Eslam, M.; Akhavan-Niaki, H. Comprehensive in silico identification of impacts of ACE2 SNPs on COVID-19 susceptibility in different populations. *Gene Reports* **2021**, *22*, 100979.
46. Brooke, G.N.; Prischi, F. Structural and functional modelling of SARS-CoV-2 entry in animal models. *Sci. Rep.* **2020**, *10*, 15917.
47. Wang, Q.; Zhang, Y.; Wu, L.; Niu, S.; Song, C.; Zhang, Z.; Lu, G.; Qiao, C.; Hu, Y.; Yuen, K.-Y.; et al. Structural and functional basis of SARS-CoV-2 entry by using human ACE2. *Cell* **2020**, *181*, 894-904.e9.

48. Bhattacharjee, M.J.; Lin, J.-J.; Chang, C.-Y.; Chiou, Y.-T.; Li, T.-N.; Tai, C.-W.; Shiu, T.-F.; Chen, C.-A.; Chou, C.-Y.; Chakraborty, P.; et al. Identifying primate ACE2 variants that confer resistance to SARS-CoV-2. *Mol. Biol. Evol.* **2021**, *38*, 2715–2731.
49. Walls, A.C.; Park, Y.-J.; Tortorici, M.A.; Wall, A.; McGuire, A.T.; Veesler, D. Structure, function, and antigenicity of the SARS-CoV-2 spike glycoprotein. *Cell* **2020**, *181*, 281-292.e6.
50. Wrapp, D.; Wang, N.; Corbett, K.S.; Goldsmith, J.A.; Hsieh, C.-L.; Abiona, O.; Graham, B.S.; McLellan, J.S. Cryo-EM structure of the 2019-nCoV spike in the prefusion conformation. *Science.* **2020**, *367*, 1260–1263.
51. Guy, J.L.; Jackson, R.M.; Jensen, H.A.; Hooper, N.M.; Turner, A.J. Identification of critical active-site residues in angiotensin-converting enzyme-2 (ACE2) by site-directed mutagenesis. *FEBS J.* **2005**, *272*, 3512–3520.
52. Towler, P.; Staker, B.; Prasad, S.G.; Menon, S.; Tang, J.; Parsons, T.; Ryan, D.; Fisher, M.; Williams, D.; Dales, N.A.; et al. ACE2 X-ray structures reveal a large hinge-bending motion important for inhibitor binding and catalysis. *J. Biol. Chem.* **2004**, *279*, 17996–18007.
53. Li, W.; Zhang, C.; Sui, J.; Kuhn, J.H.; Moore, M.J.; Luo, S.; Wong, S.K.; Huang, I.C.; Xu, K.; Vasilieva, N.; et al. Receptor and viral determinants of SARS-coronavirus adaptation to human ACE2. *EMBO J.* **2005**, *24*, 1634–1643.
54. Rowland, R.; Brandariz-Nuñez, A. Analysis of the role of N-linked glycosylation in cell surface expression, function, and binding properties of SARS-CoV-2 receptor ACE2. *Microbiol. Spectr.* **2021**, *9*, e0119921.
55. Mehdipour, A.R.; Hummer, G. Dual nature of human ACE2 glycosylation in binding to SARS-CoV-2 spike. *Proc. Natl. Acad. Sci.* **2021**, *118*, e2100425118.
56. Benetti, E.; Tita, R.; Spiga, O.; Ciolfi, A.; Birolo, G.; Bruselles, A.; Doddato, G.; Giliberti, A.; Marconi, C.; Musacchia, F.; et al. ACE2 gene variants may underlie interindividual variability and susceptibility to COVID-19 in the Italian population. *Eur. J. Hum. Genet.* **2020**, *28*, 1602–1614.
57. Han, P.; Su, C.; Zhang, Y.; Bai, C.; Zheng, A.; Qiao, C.; Wang, Q.; Niu, S.; Chen, Q.; Zhang, Y.; et al. Molecular insights into receptor binding of recent emerging SARS-CoV-2 variants. *Nat. Commun.* **2021**, *12*, 6103.
58. Moss, D.L.; Rappaport, J. SARS-CoV-2 Beta variant substitutions alter spike glycoprotein receptor binding domain structure and stability. *J. Biol. Chem.* **2021**, *297*, 101371.
59. Su, E.W.; Lin, J.Y.; Kane, L.P. TIM-1 and TIM-3 proteins in immune regulation.

Cytokine **2008**, *44*, 9–13.

60. Kuchroo, V.K.; Dardalhon, V.; Xiao, S.; Anderson, A.C. New roles for TIM family members in immune regulation. *Nat. Rev. Immunol.* **2008**, *8*, 577–580.
61. Rennert, P.D. Novel roles for TIM-1 in immunity and infection. *Immunol. Lett.* **2011**, *141*, 28–35.
62. Kachko, A.; Costafreda, M.I.; Zubkova, I.; Jacques, J.; Takeda, K.; Wells, F.; Kaplan, G.; Major, M.E. Determinants in the Ig variable domain of human HAVCR1 (TIM-1) are required to enhance hepatitis C virus entry. *J. Virol.* **2018**, *92*, 1–15.
63. Kondratowicz, A.S.; Lennemann, N.J.; Sinn, P.L.; Davey, R.A.; Hunt, C.L.; Moller-Tank, S.; Meyerholz, D.K.; Rennert, P.; Mullins, R.F.; Brindley, M.; et al. T-cell immunoglobulin and mucin domain 1 (TIM-1) is a receptor for Zaire ebolavirus and Lake Victoria marburgvirus. *Proc. Natl. Acad. Sci.* **2011**, *108*, 8426–8431.
64. Kobayashi, N.; Karisola, P.; Peña-Cruz, V.; Dorfman, D.M.; Jinushi, M.; Umetsu, S.E.; Butte, M.J.; Nagumo, H.; Chernova, I.; Zhu, B.; et al. TIM-1 and TIM-4 glycoproteins bind phosphatidylserine and mediate uptake of apoptotic cells. *Immunity* **2007**, *27*, 927–940.
65. Amara, A.; Mercer, J. Viral apoptotic mimicry. *Nat. Rev. Microbiol.* **2015**, *13*, 461–469.
66. Moller-Tank, S.; Maury, W. Phosphatidylserine receptors: Enhancers of enveloped virus entry and infection. *Virology* **2014**, *468–470*, 565–580.
67. Brunton, B.; Rogers, K.; Phillips, E.K.; Brouillette, R.B.; Bouls, R.; Butler, N.S.; Maury, W. TIM-1 serves as a receptor for Ebola virus in vivo, enhancing viremia and pathogenesis. *PLoS Negl. Trop. Dis.* **2019**, *13*, e0006983.
68. Younan, P.; Iampietro, M.; Nishida, A.; Ramanathan, P.; Santos, R.I.; Dutta, M.; Lubaki, N.M.; Koup, R.A.; Katze, M.G.; Bukreyev, A. Ebola virus binding to Tim-1 on T lymphocytes induces a cytokine storm. *MBio* **2017**, *8*, e00845-17.
69. Chu, L.-W.; Yang, C.-J.; Peng, K.-J.; Chen, P.-L.; Wang, S.-J.; Ping, Y.-H. TIM-1 as a signal receptor triggers dengue virus-induced autophagy. *Int. J. Mol. Sci.* **2019**, *20*, 4893.
70. Moller-Tank, S.; Albritton, L.M.; Rennert, P.D.; Maury, W. Characterizing functional domains for TIM-mediated enveloped virus entry. *J. Virol.* **2014**, *88*, 6702–6713.
71. Moller-Tank, S.; Kondratowicz, A.S.; Davey, R.A.; Rennert, P.D.; Maury, W. Role of the phosphatidylserine receptor TIM-1 in enveloped-virus entry. *J. Virol.*

2013, *87*, 8327–8341.

72. Kim, H.Y.; Eyheramonho, M.B.; Pichavant, M.; Gonzalez Cambaceres, C.; Matangkasombut, P.; Cervio, G.; Kuperman, S.; Moreiro, R.; Konduru, K.; Manangeeswaran, M.; et al. A polymorphism in TIM1 is associated with susceptibility to severe hepatitis A virus infection in humans. *J. Clin. Invest.* **2011**, *121*, 1111–1118.
73. Biasin, M.; Sironi, M.; Saulle, I.; Pontremoli, C.; Garziano, M.; Cagliani, R.; Trabattoni, D.; Lo Caputo, S.; Vichi, F.; Mazzotta, F.; et al. A 6-amino acid insertion/deletion polymorphism in the mucin domain of TIM-1 confers protections against HIV-1 infection. *Microbes Infect.* **2017**, *19*, 69–74.
74. Niu, J.; Jiang, Y.; Xu, H.; Zhao, C.; Zhou, G.; Chen, P.; Cao, R. TIM-1 promotes Japanese encephalitis virus entry and infection. *Viruses* **2018**, *10*, 630.
75. Kirui, J.; Abidine, Y.; Lenman, A.; Islam, K.; Gwon, Y.D.; Lasswitz, L.; Evander, M.; Bally, M.; Gerold, G. The phosphatidylserine receptor tim-1 enhances authentic chikungunya virus cell entry. *Cells* **2021**, *10*, 1828.
76. Kuroda, M.; Fujikura, D.; Noyori, O.; Kajihara, M.; Maruyama, J.; Miyamoto, H.; Yoshida, R.; Takada, A. A polymorphism of the TIM-1 IgV domain: Implications for the susceptibility to filovirus infection. *Biochem. Biophys. Res. Commun.* **2014**, *455*, 223–228.
77. Freeman, G.J.; Casasnovas, J.M.; Umetsu, D.T.; DeKruyff, R.H. TIM genes: A family of cell surface phosphatidylserine receptors that regulate innate and adaptive immunity. *Immunol. Rev.* **2010**, *235*, 172–189.
78. Santiago, C.; Ballesteros, A.; Martínez-Muñoz, L.; Mellado, M.; Kaplan, G.G.; Freeman, G.J.; Casasnovas, J.M. Structures of T cell immunoglobulin mucin protein 4 show a metal-ion-dependent ligand binding site where phosphatidylserine binds. *Immunity* **2007**, *27*, 941–951.
79. Santiago, C.; Ballesteros, A.; Tami, C.; Martínez-Muñoz, L.; Kaplan, G.G.; Casasnovas, J.M. Structures of T cell immunoglobulin mucin receptors 1 and 2 reveal mechanisms for regulation of immune responses by the TIM receptor family. *Immunity* **2007**, *26*, 299–310.
80. Yuan, S.; Cao, L.; Ling, H.; Dang, M.; Sun, Y.; Zhang, X.; Chen, Y.; Zhang, L.; Su, D.; Wang, X.; et al. TIM-1 acts a dual-attachment receptor for ebolavirus by interacting directly with viral GP and the PS on the viral envelope. *Protein Cell* **2015**, *6*, 814–824.
81. Ensembl genome browser homepage Available online: http://www.ensembl.org/index.html (accessed on Aug 10, 2022).

82. National Centre for Biotechnological Information SNP Available online: https://www.ncbi.nlm.nih.gov/snp/ (accessed on Aug 10, 2022).
83. Ensembl Pathogenicity predictions Available online: https://grch37.ensembl.org/info/genome/variation/prediction/protein_function.html (accessed on Aug 10, 2022).
84. Messaoudi, I.; Amarasinghe, G.K.; Basler, C.F. Filovirus pathogenesis and immune evasion: Insights from Ebola virus and Marburg virus. *Nat. Rev. Microbiol.* 2015, *13*, 663–676.
85. Ly, H. Differential immune responses to New World and Old World mammalian arenaviruses. *Int. J. Mol. Sci.* **2017**, *18*, 1040.
86. Yoshida, R.; Igarashi, M.; Ozaki, H.; Kishida, N.; Tomabechi, D.; Kida, H.; Ito, K.; Takada, A. Cross-protective potential of a novel monoclonal antibody directed against antigenic site B of the hemagglutinin of influenza A viruses. *PLoS Pathog.* **2009**, *5*, e1000350.
87. Waanders, F.; van Timmeren, M.M.; Stegeman, C.A.; Bakker, S.J.L.; van Goor, H. Kidney injury molecule-1 in renal disease. *J. Pathol.* **2010**, *220*, 7–16.
88. Schweigert, O.; Dewitz, C.; Möller-Hackbarth, K.; Trad, A.; Garbers, C.; Rose-John, S.; Scheller, J. Soluble T cell immunoglobulin and mucin domain (TIM)-1 and -4 generated by a disintegrin and metalloprotease (ADAM)-10 and -17 bind to phosphatidylserine. *Biochim. Biophys. Acta - Mol. Cell Res.* **2014**, *1843*, 275–287.
89. Zhang, X.; Liang, C.; Wang, H.; Guo, Z.; Rong, H.; Pan, J.; Li, W.; Pei, R.; Chen, X.; Zhang, Z.; et al. T-cell immunoglobulin and mucin domain 1 (TIM-1) is a functional entry factor for tick-borne encephalitis virus. *MBio* **2022**, *13*, e02860-21.
90. Zhang, M.; Wang, X.; Hu, L.; Zhang, Y.; Zheng, H.; Wu, H.; Wang, J.; Luo, L.; Xiao, H.; Qiao, C.; et al. TIM-1 augments cellular entry of Ebola virus species and mutants, which is blocked by recombinant TIM-1 protein. *Microbiol. Spectr.* **2022**, *10*, e0221221.
91. Tami, C.; Silberstein, E.; Manangeeswaran, M.; Freeman, G.J.; Umetsu, S.E.; DeKruyff, R.H.; Umetsu, D.T.; Kaplan, G.G. Immunoglobulin A (IgA) is a natural ligand of hepatitis A virus cellular receptor 1 (HAVCR1), and the association of IgA with HAVCR1 enhances virus-receptor interactions. *J. Virol.* **2007**, *81*, 3437–3446.
92. Lee, J.; Phong, B.; Egloff, A.M.; Kane, L.P. TIM polymorphisms—genetics and function. *Genes Immun.* **2011**, *12*, 595–604.

93. Chae, S.-C.; Song, J.-H.; Heo, J.-C.; Lee, Y.-C.; Kim, J.-W.; Chung, H.-T. Molecular variations in the promoter and coding regions of human Tim-1 gene and their association in Koreans with asthma. *Hum. Immunol.* **2003**, *64*, 1177–1182.
94. Chae, S.-C.; Park, Y.-R.; Song, J.-H.; Shim, S.-C.; Yoon, K.-S.; Chung, H.-T. The polymorphisms of Tim-1 promoter region are associated with rheumatoid arthritis in a Korean population. *Immunogenetics* **2005**, *56*, 696–701.
95. Perera-Lecoin, M.; Meertens, L.; Carnec, X.; Amara, A. Flavivirus entry receptors: An update. *Viruses* **2013**, *6*, 69–88.
96. Brouillette, R.B.; Phillips, E.K.; Patel, R.; Mahauad-Fernandez, W.; Moller-Tank, S.; Rogers, K.J.; Dillard, J.A.; Cooney, A.L.; Martinez-Sobrido, L.; Okeoma, C.; et al. TIM-1 mediates dystroglycan-independent entry of Lassa virus. *J. Virol.* **2018**, *92*, e00093-18.

Summary in Japanese (和文要旨)

近年、新型コロナウイルスやエボラウイルスなどによる新興感染症の発生が世界的に公衆衛生上の問題となっている。これらのウイルスは重篤な病態を引き起こす病原体として知られる一方で、無症状もしくは軽症で経過する症例も多く存在することが分かってきた。その要因の 1 つとして、宿主因子の遺伝子多型がウイルスへの感受性や重症度に関与している可能性が考えられている。ウイルスが宿主細胞に感染する際、ウイルス粒子は細胞膜上の受容体に結合し細胞内への侵入を開始する。よって、宿主受容体の遺伝子多型は、ウイルスの細胞侵入効率に影響を与えうると考えられる。本研究では、ウイルスの細胞侵入過程に影響を及ぼす宿主細胞受容体の一塩基変異（SNV）に着目した。

コロナウイルス（CoVs）科に属する重症急性呼吸器症候群コロナウイルス（SARS-CoV）および SARS-CoV-2 はヒトに重篤な肺炎を引き起こすことが知られている。これら CoVs のスパイク蛋白質（S 蛋白質）は、宿主細胞膜上のアンジオテンシン変換酵素 2（ACE2）を主要な受容体として細胞内に侵入する。これまでに、ACE2 の 29 個の SNV が SARS-CoV-2 の S 蛋白質との結合親和性に影響を与えることが示唆されていた。しかし、これらの SNV が実際に SARS-CoV および SARS-CoV-2 の細胞侵入効率に影響を与えるか否かは明らかになっていなかった。第一章では、ACE2 の SNV が SARS-CoV および SARS-CoV-2 の細胞侵入効率に与える影響を *in vitro* で解析した。これらの CoVs に対して低い感受性を示す HEK293T 細胞に、ヒト由来の野生型 ACE2 または各 SNV 変異を導入した ACE2 遺伝子を一過性に発現させ、水疱性口内炎ウイルス（VSIV）の G 蛋白質を S 蛋白質に置換したシュードタイプウイルスに対する感受性を比較した。その結果、H505R 変異体は両方の CoVs の感染性を有意に増強する事が示唆された。また、SARS-CoV の感染性は、G352V および Y515C 変異体によって増強、D355N 変異体によって減弱することが示唆された。さらに、SARS-CoV-2 の変異株（Alpha、Beta、Gamma および Delta 株）の S 蛋白質について同様の解析を行ったところ、E35K 変異体が Beta および Gamma 株の感染性のみ有意に低下させることが分かった。この結果は、SNV が与える影響は SARS-CoV-2 の変異株間で僅かに異なることを示唆している。以上の結果より、ACE2 の SNV が SARS-CoV および SARS-CoV-2 に対する細胞感受性に影響を与える可能性が示された。

Human T-cell immunoglobulin mucin 1（hTIM-1）は ウイルス吸着因子として様々なエンベロープウイルスの感染を増強することが知られている。 hTIM-1 の IgV domain に存在する 3 つのループ構造 (BC、CC'および FG ループ)が、エボラウイルス（EBOV）のエンベロープ内に存在するホスファチジルセリン（PS）および表面糖蛋白質（GP）に結合することが分かっている。第二章では、これらの

ループ構造内に存在するSNV変異がフィロウイルスおよびアレナウイルスに対する細胞感受性に与える影響を解析した。まず、公共の遺伝子データベースでSNVの配列情報を検索し、3つのループ構造内にアミノ酸置換を伴う35か所のSNV変異を見出した。これら35個のSNV変異体を作出し、野生型hTIM-1または各SNV変異を導入したhTIM-1遺伝子をHEK293T細胞に一過性に発現させた。これらのhTIM-1発現細胞に、3種類のフィロウイルス（EBOV、マールブルグウイルス [MARV]、ヨビュウイルス [LLOV]）および2種類のアレナウイルス（フニンウイルス [JUNV]、ラッサウイルス [LASV]）のGPを持つシュードタイプVSIVを感染させ感受性を比較した。その結果、7個のSNV（L34P、C46W、W47R、C57S、H109P、N114SおよびD115G）はLASVを除く5種類のウイルスに共通してhTIM-1発現による感染増強を有意に減弱させることが分かった。また、I124T変異体はEBOV、MARV、LLOVおよびJUNVのGP、R110CおよびG111R変異体はEBOV、LLOVおよびJUNVのGP、V62I変異体はJUNVのGPをもつシュードタイプウイルスの感染性を減弱させた。以上の結果より、SNV変異体がウイルスの細胞侵入へ与える影響は、GPによって違いがあることが分かった。さらに、EBOVの感染性を有意に減弱すると考えられた各SNV変異を含む可溶性hTIM-1蛋白質を作出し、シュードタイプウイルスを用いて中和活性を解析した結果、野生型hTIM-1と比較して中和活性が有意に低下することが分かった。ウイルスの感染性を減弱させた11個のSNVのうち、5個のSNVのアミノ酸変異箇所はPS結合領域に位置し、6個のSNVの変異箇所はこの部位から離れた領域に位置していた。これらの結果から、hTIM-1分子の11カ所のSNV変異は、ウイルスエンベロープ上のPSおよびGPとの相互作用を低下させ、フィロウイルスおよびアレナウイルスに対する細胞感受性に影響を与える可能性が示唆された。

本論文により、宿主細胞受容体の遺伝子多型がウイルスの細胞侵入効率に影響を与えうることが示唆された。これらの新しい知見は、個体間レベルでのウイルスに対する感受性あるいは病態の違いに関与する宿主因子の解明に役立つと期待される。また、本研究の成果は新型コロナウイルスおよび出血熱ウイルスの細胞侵入機構および受容体分子との相互作用メカニズムの詳細な解明にも貢献することが期待される。今後、全ゲノム解析によるヒトの遺伝的多様性に関するデータの蓄積とともに、ウイルスへの感受性や重症化に関わる遺伝子多型の同定、地域または人種間の遺伝子多型の違いとウイルス感染症の流行状況との関連等についてさらなる研究が必要である。